PONTIFICIA UNIVERSIDAD CATÓLICA DEL PERÚ

ESCUELA DE POSGRADO

Geometric Phases in Polarization Mixed States

A thesis in candidacy for the degree of Master of Science in Physics presented by:

Diego Eduardo Barberena Helfer

Advisor:
Prof. Francisco de Zela

Jury:
Prof. Eduardo Massoni
Prof. Hernán Castillo

Lima, 2016

Fases geométricas en estados mixtos de polarización

Diego Eduardo Barberena Helfer

Propuesto para el grado de Magíster en Física

Resumen

Debido a la generalidad de su formulación, las fases geométricas han sido objeto de constantes investigaciones en áreas muy diversas y han llevado a muchos desarrollos, tanto en aplicaciones como en trabajo teórico. Esta tesis se incluye dentro de las investigaciones experimentales y se enfoca en las fases geométricas que aparecen al manipular el grado de libertad de polarización. Se divide en dos partes. La primera se centra en los aspectos teóricos esenciales que definen y relacionan los estados mixtos de polarización con la luz láser parcialmente polarizada, y en las propiedades de las fases geométricas que aparecen en los primeros. La segunda parte presenta dos arreglos experimentales, uno que genera estados polarización y uno que permite medir la fase geométrica adquirida por dichos estados después de alguna evolución unitaria. El primero otorga un control casi arbitrario del estado de polarización de la luz láser que deja el arreglo y, con una ligera modificación, puede utilizarse en fotones individuales con casi idéntica efectividad. El segundo utiliza al primero para generar estados mixtos de polarización y luego los somete a distintas evoluciones. Las fases geométricas adquiridas son entonces determinadas mediante su relación con las fases de Pancharatnam correspondientes, que son cantidades directamente observables. Si bien hubo casos en los que la fase no se pudo determinar debido a su sensibilidad a errores experimentales, en aquellas mediciones en las que se pudo obtener un valor experimental este se ajustó muy bien a la predicción teórica.

Geometric Phases in Polarization Mixed States

Diego Eduardo Barberena Helfer

Presented towards a Master's degree in Physics

Abstract

Because of the generality of their formulation, geometric phases have been a subject of continuous research in very different areas and have led to various developments, both in applications and in theoretical work. This thesis falls in the line of experimental investigations and focuses, in particular, in the geometric phases that appear in mixed states of the polarization degree of freedom. It consists of two parts. The first one deals with the essential theoretical aspects that define and relate polarization mixed states with partially polarized laser light, and with the properties of geometric phases that show up in the mixed states in question. The second one presents two experimental setups, designed to prepare polarization states and to generate and measure geometric phases, respectively. The first array provides almost arbitrary control over the generated polarization state and can be modified to operate on single photons with the same effectiveness. The second array uses the first one to generate mixed states and then subjects them to different evolutions, thereby acquiring geometric phases. The latter are then measured by relating them to the corresponding Pancharatnam phases, which are directly observable quantities and the results are contrasted with the theoretical predictions. Even though not all intended points could be measured because of the sensibility of the phase to experimental errors, a very good agreement was found in all cases in which the phase could be determined.

Acknowledgments

This work has been completed (at last) thanks to all the persons with which I have had the pleasure to share some time on this planet. Though I cannot name each and every one of them, certainly there are people I would like to mention.
My mother Danitza, my father Eduardo and my sister Ariana have been a constant support without which this work would have taken considerably longer (if not forever). A very big Thank You to you for filling my nights (which were, at times, the only moments in which I was able to see you) with the joy and lightheartedness of the family dinners.
I am also greatly indebted to Professor Francisco de Zela for his terrific guidance as teacher and advisor in this small attempt at delving into this marvelous subject called physics. His vision of creating the Quantum Optics group is the reason I was able to do this work.
I would also like to thank Professor Enrique Solano, Julen Simon and Mikel Sanz for giving me the opportunity to participate in various projects with them and showing me the power of trusting one's own ideas.
I also thank you, Fortune, for those cherishable moments that I have lived with you and for making lighter the last part of the quest, which is the writing of this thesis. My friends have certainly played an important part too. Diana and Giancarlo, thanks for your unconditional friendship during these two years. I also thank Yonny, Omar and Rafael for the shared hours of darkness in the lab during the measurements. Bonds definitely tighten in that situation.
I thank all the people I have not mentioned but have nevertheless had impact on this work. I also thank CONCYTEC/FONDECYT for financial support.

Published Material in this Thesis

Results contained in this Thesis have been published in the following journal articles:

D. Barberena, G. Gatti, and F. D. Zela, *Experimental demonstration of a secondary source of partially polarized states*, J. Opt. Soc. Am. A **32** (2015), 697-700.

D. Barberena, O. Ortíz, Y. Yugra, R. Caballero, and F. De Zela, *All-optical polarimetric generation of mixed-state single-photon geometric phases*, Phys. Rev. A **93** (2016), 013805.

Contents

List of Figures

Chapter 1

Introduction

Geometric phases have been a subject of intense research since their discovery in 1984 [1]. From then on, theoretical generalizations applicable to ever more general physical situations (both classical and quantum) have been developed and relations with themes as diverse as gauge theory, topology, condensed matter physics and Hamiltonian dynamics, to name a few, have been established. Implications for quantum computing have also been theorized since [2].

Experimental investigations have gone hand in hand with theoretical developments. Direct measurements have been done in several platforms: superconducting circuits [3], ultracold neutrons [4], photon polarization [5], etc. Several of their properties, such as their response to noise, have also been tested [6]. Furthermore, geometric phases have also been used as tools to, for example, asses the conductance properties of some materials [7], or to create artificial magnetic fields acting on atoms [8].

In view of all these different approaches to the subject, this work centers on one of them, namely the experimental measurement of geometric phases that arise in photon polarization. It should therefore be considered as the natural continuation of [5], one that tries to extend its results to the realm of polarization mixed states. Even though experiments of these kind have already been done [9], we can address these polarization mixed states with greater generality and we try to demonstrate this capability in the experiments we have performed.

This Thesis is organized as follows: in Chapter 2 we revise the concepts of mixed states, how do they arise in the polarization degree of freedom and how are they understood in terms of the standard quantum description of the Electromagnetic Field. A parallel is also made with the polarization of classical lasers so that the sequence of experiments presented in this Thesis can be better understood. Chapter 3 deals properly with subject of phases in general (geometric and otherwise),

and a summary of their main properties is presented. In Chapter 4 we present our main results: the sequence of experiments that allowed the preparation of arbitrary polarization mixed states and the subsequent generation and measurement of geometric phases in them. We close with a summary of this work and our conclusions in Chapter 5.

Chapter 2

Mixed states in polarization optics

In this chapter, the most important properties of mixed states are revised. Polarization mixed states are then discussed in the context of single-photon states: how do they arise and what are their properties. The partial polarization properties of a laser source are then discussed and the known parallelism between both systems (single photon and laser polarization) is reviewed because it will be of use in the experiment.

2.1 General overview of mixed states

Mixed states are ubiquitous in physics. No real system (except perhaps for the universe itself) is perfectly prepared nor completely isolated. Either there is imperfect knowledge about its quantum state or it is entangled with another system, in which case a pure state description will not suffice. The latter can only be used when certain approximations regarding the environment and state of knowledge of the observer can be made.

The description of mixed states is done with density matrices or operators. They are constructed as follows: if there is imperfect knowledge about the quantum state of the system, i.e. if the system is known to be in state $|\psi_i\rangle$ with probability p_i, the density operator is shown in (2.1).

$$\rho = \sum_i p_i |\psi_i\rangle\langle\psi_i| \tag{2.1}$$

If the system is entangled with other systems, the prescription is (2.2), where $|\Psi\rangle_{S+E}$ is the full quantum state of the system plus anything it is entangled with (denoted

by E) and tr_E is a trace with respect to the degrees of freedom of these other things.

$$\rho = \mathrm{tr}_E(|\Psi\rangle_{S+E}\langle\Psi|_{S+E}) \tag{2.2}$$

In any case, if the larger system is already described by a density matrix ρ_{S+E}, the rule generalizes straightforwardly to (2.3).

$$\rho = \mathrm{tr}_E(\rho_{S+E}) \tag{2.3}$$

The most important properties of density matrices are listed in (2.4). Demonstrations can be found in any standard text in Quantum Mechanics.

$$\begin{aligned}
\rho^\dagger &= \rho \\
tr(\rho) &= 1 \\
tr(\rho^2) &\leq 1 \\
P_{|k\rangle} &= \text{Probability of detecting the system in state } |k\rangle \\
&= \langle k|\rho|k\rangle \\
\langle O\rangle &= \text{Mean value of observable } O \text{ when measuring state } \rho \\
&= \mathrm{tr}(O\rho)
\end{aligned} \tag{2.4}$$

2.2 Polarization mixed states

2.2.1 Single photon polarization

To study polarization mixed states, the first thing to do is to identify the relevant pure states. In the case of the electromagnetic (EM) field, the standard basis vectors used to construct quantum states are denoted by the occupation number of each mode of the field. In turn, each mode is labelled by the momentum and polarization of the photons it can contain. There's the vacuum (all occupation numbers equal to zero)(2.5), for example, and one-photon states (all occupation numbers equal to zero except for one equal to one)(2.6).

$$|vac\rangle = ...|0\rangle_{\boldsymbol{k_1},H}|0\rangle_{\boldsymbol{k_1},V}|0\rangle_{\boldsymbol{k_2},H}|0\rangle_{\boldsymbol{k_2},V}|0\rangle_{\boldsymbol{k_3},H}... \tag{2.5}$$

$$|\boldsymbol{k_2}, H\rangle = ...|0\rangle_{\boldsymbol{k_1},H}|0\rangle_{\boldsymbol{k_1},V}|1\rangle_{\boldsymbol{k_2},H}|0\rangle_{\boldsymbol{k_2},V}|0\rangle_{\boldsymbol{k_3},H}... \tag{2.6}$$

To avoid the cumbersome repetition of irrelevant modes of the EM field (whose occupation number will always be zero), the shorthand notation shown in (2.6) will be employed. There, a ket such as $|\boldsymbol{k_2}, H\rangle$ denotes a configuration of the EM field in

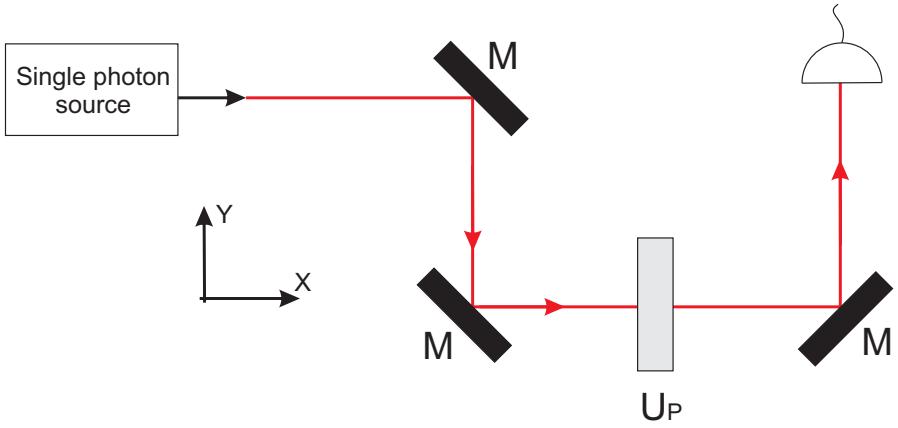

Figure 2.1: Photons travel only along one path, so the polarization label suffices. The M's stand for mirrors and U_P is a generic polarization transformation.

which there is one photon present with momentum $\boldsymbol{k_2}$ and H polarization (measured with respect to a specified direction in the plane perpendicular to $\boldsymbol{k_2}$). Since most of the work will be done with one-photon states, this will be enough.

The momentum label will be omitted when a single beam is considered since no confusion can arise, even if the momentum of the photon changes (see Fig.(2.1)). In the case of an interferometer, there will be times at which superpositions of states with different momenta are present (though while still working with one photon states). States will then be labelled by the direction in which the photon is propagating (along with its polarization) with respect to some coordinate axes. Situation II in Fig.(2.2) illustrates this case. The state is written in (2.7) and the action of most optical elements (beam splitter, mirrors, wave plates, etc.) can be described very succinctly in terms of these labels (see [10]).

$$|\psi\rangle \propto |\boldsymbol{k_1}, H\rangle + |\boldsymbol{k_2}, H\rangle = |X, H\rangle + |Y, H\rangle \tag{2.7}$$

Situation III involves states with the same momentum but non-overlapping in space. An exhaustive description which makes manifest the difference between the beams would require the use of wavepackets and superpositions of states like (2.6) with different transverse momenta, but since one is usually interested in the outputs of the interferometer, no special notation will be devised and this configuration will not be mentioned again.

When talking about a single photon polarization mixed state, what is meant are configurations of the EM field that are described by a density matrix of the form of

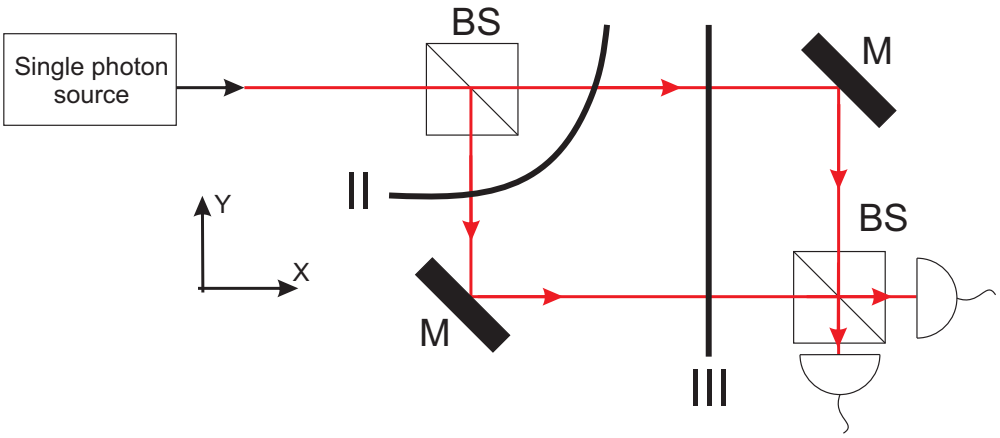

Figure 2.2: Two situations are shown. II involves a superposition of one-photon states that propagate in different directions and the state is denoted in (2.7). III involves superpositions of one-photon states propagating in the same direction. Distinction between the arms is related to wave packet localization, which necessarily involves many states like (2.6).

(2.8).

$$\begin{aligned}\rho &= a|\boldsymbol{k},H\rangle\langle\boldsymbol{k},H| + \gamma|\boldsymbol{k},H\rangle\langle\boldsymbol{k},V| + \gamma^*|\boldsymbol{k},V\rangle\langle\boldsymbol{k},H| + (1-a)|\boldsymbol{k},V\rangle\langle\boldsymbol{k},V| \\ &= a|H\rangle\langle H| + \gamma|H\rangle\langle V| + \gamma^*|V\rangle\langle H| + (1-a)|V\rangle\langle V| \end{aligned} \tag{2.8}$$

(2.8) describes the presence of one photon traveling in a certain direction without a sharp polarization. The presence of only one direction should be stressed. If $|\boldsymbol{k},V\rangle$ were replaced by $|\boldsymbol{k'},V\rangle$, the state would be a mixture of EM field configurations with a photon traveling in different directions correlated with their polarization. Of course, if two detectors: (1) collected photons coming with $\boldsymbol{k}$ and $\boldsymbol{k}'$ respectively, (2) did polarization analysis such that both beams were projected into the same polarization state and (3) summed their individual counts (thereby forgetting from which path the photons came), the results would be accurately described by (2.8). Physically, however, it is a very different situation.

(2.8) can also be obtained in more general (and realistic) cases. Instead of working with states such as (2.6), the modes of the EM field which are not $(\boldsymbol{k},H)$ nor $(\boldsymbol{k},V)$ can be in any other state. (2.8) results, then, from tracing with respect to these other modes (leaving aside, perhaps, modes that can interact with the original ones via beam splitters and such).

In any case, the state ρ can be taken directly from (2.8) and analyzed. Since it is a hermitian operator in a two-dimensional space, it has a matrix representation

spanned by the unit matrix and the Pauli matrices.

$$\rho = \frac{1}{2} + \frac{1}{2}\boldsymbol{S}\cdot\boldsymbol{\sigma} \tag{2.9}$$

The requirement $\mathrm{tr}(\rho^2) \leq 1$ implies $|\boldsymbol{S}| \leq 1$. This means that the three-dimensional vector $\boldsymbol{S}$ (called the Stokes vector) lies within the unit sphere in $\mathbb{R}^3$. Because ρ and $\boldsymbol{S}$ are in a one to one correspondence, the tip of $\boldsymbol{S}$ can be identified with ρ. Therefore, any kind of transformation on ρ can be visualized geometrically in this sphere, commonly called the Poincaré sphere, which is analogous to the Bloch sphere for spin $\frac{1}{2}$. Pure states lie at the surface, while the most incoherent mixture ($\rho = \frac{1}{2}$) rests at the origin. Partially polarized states lie between them.
By diagonalizing (2.9) one obtains (2.10), where $\boldsymbol{S} = P\hat{\boldsymbol{n}}$ (with $P \in [0,1]$ and $\hat{\boldsymbol{n}}\cdot\hat{\boldsymbol{n}} = 1$) and $|\hat{\boldsymbol{n}}\rangle$ is a pure state whose Stokes vector lies in the direction $\hat{\boldsymbol{n}}$ in the sphere.

$$\rho = \frac{1+P}{2}|\hat{\boldsymbol{n}}\rangle\langle\hat{\boldsymbol{n}}| + \frac{1-P}{2}|-\hat{\boldsymbol{n}}\rangle\langle-\hat{\boldsymbol{n}}| \tag{2.10}$$

When acting with a unitary operator on ρ, the degree of polarization, P (equal to $\sqrt{1-4\det\rho}$), is kept fixed while the kets $|\hat{\boldsymbol{n}}\rangle$ and $|-\hat{\boldsymbol{n}}\rangle$ change. The result of $U|\hat{\boldsymbol{n}}\rangle\langle\hat{\boldsymbol{n}}|U^\dagger$ can be described as a rotation in the Poincaré sphere: $U|\hat{\boldsymbol{n}}\rangle\langle\hat{\boldsymbol{n}}|U^\dagger = |\boldsymbol{R_U}\cdot\hat{\boldsymbol{n}}\rangle\langle\boldsymbol{R_U}\cdot\hat{\boldsymbol{n}}|$, where R_U is a rotation matrix in $\mathbb{R}^3$ that depends on U.

2.2.2 Laser polarization

The classical analog of the above situation would be a partially polarized laser source. The main difference between both is that partial polarization is a property of the quantum state itself in the former and of the expectation value of the electric field operator in the latter. Nevertheless, their mathematical description is identical (modulo some nomenclature). There exists for this case an object analogous to (2.9) called the polarization matrix [11] and we shall show how it arises.
The quantum state of a horizontally polarized EM field produced by a single-mode laser working well above threshold can be described by a coherent state (2.11) with an extremely large mean number of photons ($\bar{n} = |\alpha|^2$).

$$\begin{aligned} |\psi\rangle &= \ldots|0\rangle^F_{\boldsymbol{k_1},H}|0\rangle^F_{\boldsymbol{k_1},V}|\alpha\rangle^C_{\boldsymbol{k_2},H}|0\rangle^F_{\boldsymbol{k_2},V}|0\rangle^F_{\boldsymbol{k_3},H}\ldots \\ |\alpha\rangle^C_{\boldsymbol{k_2},H} &= e^{-|\alpha|^2/2}\sum_{n=0}\frac{\alpha^n}{\sqrt{n!}}|n\rangle^F_{\boldsymbol{k_2},H} \end{aligned} \tag{2.11}$$

The F and C superscripts mean Fock and Coherent, respectively, and are used to distinguish these two very different kinds of states. Note that (2.11) really describes

a non-localized source with both infinite space and time extent and it is, therefore, an approximation. For now it suffices, but situations will be encountered in which this assumption will be relaxed.

A laser source in the same momentum mode ($\boldsymbol{k}_2$) but another polarization is represented as (2.12).

$$|\psi'\rangle = ...|0\rangle^F_{\boldsymbol{k_1},H}|0\rangle^F_{\boldsymbol{k_1},V}|\alpha\rangle^C_{\boldsymbol{k_2},H}|\beta\rangle^C_{\boldsymbol{k_2},V}|0\rangle^F_{\boldsymbol{k_3},H}... \tag{2.12}$$

It is not made from the superposition of states like (2.11), as happens in the single photon case but remains a product state with respect to the EM field modes.

What is additive, though, is the expectation value of the (Heisenberg picture) electric field operator (2.13).

$$\boldsymbol{E}_{\boldsymbol{x}}(t) = \int_{\boldsymbol{k}} f_{\boldsymbol{k}} e^{i\boldsymbol{k}\cdot\boldsymbol{x}-i\omega_{\boldsymbol{k}}t}(a_{\boldsymbol{k},H}\hat{\boldsymbol{\epsilon}}_{\boldsymbol{k},H} + a_{\boldsymbol{k},V}\hat{\boldsymbol{\epsilon}}_{\boldsymbol{k},V}) + h.c. \tag{2.13}$$

$a_{\boldsymbol{k},H}$ is a destruction operator that destroys a photon of momentum $\boldsymbol{k}$ and H polarization, $\hat{\boldsymbol{\epsilon}}_{\boldsymbol{k},H}$ is a unit vector pointing in the H direction (defined with respect to $\boldsymbol{k}$), $f_{\boldsymbol{k}}$ includes some factors related to normalization and h.c. stands for hermitian conjugate.

For example, the expectation value of (2.13) with respect to (2.11) is (2.14) and with respect to (2.12) is (2.15).

$$\langle \boldsymbol{E}_{\boldsymbol{x}}(t)\rangle_{\psi} = f_{\boldsymbol{k}_2} e^{i\boldsymbol{k_2}\cdot\boldsymbol{x}-i\omega_{\boldsymbol{k}_2}t}\alpha\hat{\boldsymbol{\epsilon}}_{\boldsymbol{k}_2,H} + c.c. \tag{2.14}$$

$$\langle \boldsymbol{E}_{\boldsymbol{x}}(t)\rangle_{\psi'} = f_{\boldsymbol{k}_2} e^{i\boldsymbol{k_2}\cdot\boldsymbol{x}-i\omega_{\boldsymbol{k}_2}t}(\alpha\hat{\boldsymbol{\epsilon}}_{\boldsymbol{k}_2,H} + \beta\hat{\boldsymbol{\epsilon}}_{\boldsymbol{k}_2,V}) + c.c. \tag{2.15}$$

The c.c. stands for complex conjugate. Because it contains no new information, the c.c. will be omitted from now on. The prefactors including $f_{\boldsymbol{k}}$ and $e^{i\boldsymbol{k}\cdot\boldsymbol{x}-i\omega_{\boldsymbol{k}}t}$ will also be omitted since they only affect calculations that take into account the exact intensity and phase of the field (when coherence is involved, for example) and all will be normalized to unit intensity (therefore $|\alpha|^2 + |\beta|^2 = 1$).

The resulting quantity is very similar to a one photon quantum state. (2.16) is the quantum state of a photon with a given polarization whereas (2.17) is the electric field of a laser with that same polarization.

$$|\phi\rangle = \alpha|\boldsymbol{k}, H\rangle + \beta|\boldsymbol{k}, V\rangle \tag{2.16}$$

$$\boldsymbol{E}^+ = \alpha\hat{\boldsymbol{\epsilon}}_{\boldsymbol{k},H} + \beta\hat{\boldsymbol{\epsilon}}_{\boldsymbol{k},V} \tag{2.17}$$

The analogy is very strong and there is the temptation to unify the descriptions by setting $|\boldsymbol{k}, H\rangle \leftrightarrow \hat{\boldsymbol{\epsilon}}_{\boldsymbol{k},H}$. If this is done, it should be remembered that they mean two very different things when referring to single photons or to lasers. In the former they are vectors in Hilbert space and in the latter they are vectors in three-dimensional space.

If the analogy is to be taken seriously, density matrices should have an analogue too. By mimicking their construction but using (2.17), a dyad is obtained. It can be represented in matrix form (2.18) where the first and second entries, be it of a column or row, stand for $\hat{\boldsymbol{\epsilon}}_{\boldsymbol{k},H}$ and $\hat{\boldsymbol{\epsilon}}_{\boldsymbol{k},V}$ components. Since the matrix entries are quadratic functions of the electric field components, they are easily connected to intensity measurements.

$$J = \begin{pmatrix} |\alpha|^2 & \alpha\beta^* \\ \alpha^*\beta & |\beta|^2 \end{pmatrix} \tag{2.18}$$

More generally, given the quantum state (of a laser) in (2.19), the expectation value of the positive frequency part of the electric field operator is calculated (2.20). Note that even taking into account spatial localization (enforced by the presence of several adequate $\alpha_{\boldsymbol{k}}$ and $\beta_{\boldsymbol{k}}$) the quantum state remains factorizable.

$$|\psi\rangle = ...|\alpha_{\boldsymbol{k_1}}\rangle^C_{\boldsymbol{k_1},H}|\beta_{\boldsymbol{k_1}}\rangle^C_{\boldsymbol{k_1},V}|\alpha_{\boldsymbol{k_2}}\rangle^C_{\boldsymbol{k_2},H}|\beta_{\boldsymbol{k_2}}\rangle^C_{\boldsymbol{k_2},V}|\alpha_{\boldsymbol{k_3}}\rangle^C_{\boldsymbol{k_3},H}... \tag{2.19}$$

$$\begin{aligned} \boldsymbol{E}^+_{\boldsymbol{x}}(t) &= \left\langle \int_{\boldsymbol{k}} f_{\boldsymbol{k}} e^{i\boldsymbol{k}\cdot\boldsymbol{x} - i\omega_{\boldsymbol{k}}t}(a_{\boldsymbol{k},H}\hat{\boldsymbol{\epsilon}}_{\boldsymbol{k},H} + a_{\boldsymbol{k},V}\hat{\boldsymbol{\epsilon}}_{\boldsymbol{k},V}) \right\rangle \\ &= \int_{\boldsymbol{k}} f_{\boldsymbol{k}} e^{i\boldsymbol{k}\cdot\boldsymbol{x} - i\omega_{\boldsymbol{k}}t}(\alpha_{\boldsymbol{k}}\hat{\boldsymbol{\epsilon}}_{\boldsymbol{k},H} + \beta_{\boldsymbol{k}}\hat{\boldsymbol{\epsilon}}_{\boldsymbol{k},V}) \end{aligned} \tag{2.20}$$

Since the laser electric field is paraxial, the only $\alpha_{\boldsymbol{k}}$ and β_k appreciably different from zero are those for which $\boldsymbol{k}$ has a very large component along a fixed direction (with an almost fixed magnitude because lasers have a very narrow spectrum) in the laboratory frame with some small components in the transverse directions. This allows the definition of global H and V directions (2.21).

$$\begin{aligned} \boldsymbol{E}^+_{\boldsymbol{x}}(t) &= \left(\int_{\boldsymbol{k}} f_{\boldsymbol{k}} e^{i\boldsymbol{k}\cdot\boldsymbol{x} - i\omega_{\boldsymbol{k}}t}\alpha_{\boldsymbol{k}} \right) \hat{\boldsymbol{\epsilon}}_H + \left(\int_{\boldsymbol{k}} f_{\boldsymbol{k}} e^{i\boldsymbol{k}\cdot\boldsymbol{x} - i\omega_{\boldsymbol{k}}t}\beta_{\boldsymbol{k}} \right) \hat{\boldsymbol{\epsilon}}_V \\ &= E^+_H(\boldsymbol{x},t)\hat{\boldsymbol{\epsilon}}_H + E^+_V(\boldsymbol{x},t)\hat{\boldsymbol{\epsilon}}_V \end{aligned} \tag{2.21}$$

This should come as no surprise since anyone who has seen a laser knows that it propagates basically in one direction and its transverse plane is a well-defined quantity. With this, the space and time dependent matrix (2.22) is constructed.

$$J_{ij}(\boldsymbol{x},t) = E^+_i(\boldsymbol{x},t)E^+_j(\boldsymbol{x},t)^* \qquad\qquad i,j = H,V \tag{2.22}$$

As it stands, (2.22) describes the instantaneous polarization state at a specific point in space. It is totally polarized by construction. However, detectors have a finite space and time resolution so they really average over a time period T and a spatial area A. The complete definition that takes this into account is (2.23).

$$J_{ij} = \frac{1}{T}\int_{t_0}^{t_0+T} dt \int_A J_{ij}(\boldsymbol{x},t)d^2\boldsymbol{x} \tag{2.23}$$

It should be clear that this integration procedure is completely analogous to (2.1). Each space-time point in the integral contributes one projector to the sum. The vector (2.21) has complex entries and while not normalized, can be considered to be a normalized vector times its modulus ($\sqrt{|E_H^+(\boldsymbol{x},t))|^2 + |E_V^+(\boldsymbol{x},t)|^2}$). The normalized vector part contributes the $|\psi_i\rangle\langle\psi_i|$ terms, while the modulus squared is the p_i. Since the different p_i sum up to $\int_{t_0}^{t_0+T} dt \int_A (|E_H^+(\boldsymbol{x},t))|^2 + |E_V^+(\boldsymbol{x},t)|^2)d^2\boldsymbol{x}$, and there is an extra $\frac{1}{T}$ factor besides the sum, a unit trace normalized polarization matrix can be defined by (2.24).

$$\rho_{ij} = \frac{\frac{1}{T}\int_{t_0}^{t_0+T} dt \int_A E_i^+(\boldsymbol{x},t)E_j^+(\boldsymbol{x},t)^* d^2\boldsymbol{x}}{\frac{1}{T}\int_{t_0}^{t_0+T} dt \int_A (|E_H^+(\boldsymbol{x},t))|^2 + |E_V^+(\boldsymbol{x},t)|^2)d^2\boldsymbol{x}} \tag{2.24}$$

Many properties follow directly (2.25) because it has been constructed in exactly the same way as a density matrix would be.

$$\begin{aligned}
\mathrm{tr}(\rho) &= 1 \\
\mathrm{tr}(\rho^2) &\leq 1 \\
\rho &= \frac{1}{2} + \frac{1}{2}\boldsymbol{S}\cdot\boldsymbol{\sigma} \\
|\boldsymbol{S}| &= P \leq 1 \\
\boldsymbol{S} &= P\hat{\boldsymbol{n}} \\
\rho &= \frac{1+P}{2}|\hat{\boldsymbol{n}}\rangle\langle\hat{\boldsymbol{n}}| + \frac{1-P}{2}|-\hat{\boldsymbol{n}}\rangle\langle-\hat{\boldsymbol{n}}|
\end{aligned} \tag{2.25}$$

The state of polarization of the laser source can be visualized in the Poincaré sphere. The graphical representation is identical, be it a quantum mixed state or a partially polarized laser state.

It is also a known fact that the representation of a specific polarization changing operation is the same both for a density matrix (one photon state) or a polarization matrix (laser state). Elements such as quarter-wave and half-wave plates are associated to unitary matrices members of SU(2) that rotate the Stokes vector in the Poincaré sphere. They act in the following way: $\rho \to U^\dagger \rho U$. On the other hand,

polarizers are represented by projection matrices that satisfy $P^2 = P$ and $P^\dagger = P$. After acting on a state ($\rho' = P\rho P$), the resulting matrix is no longer trace normalized to unity. In one photon states, the magnitude of the trace is the probability that the photon is measured in the state into which the polarizer projects, whereas in laser states it is the intensity of the light transmitted through the element. The resulting matrix, after trace normalizing it, will now describe either a photon or a laser with the polarization given by the polarizer.

Chapter 3

Phases

In this chapter, the different kinds of phases that have appeared in the literature are described. The experimentally-motivated Pancharatnam phase and theoretically-motivated Berry/geometric phase are defined and the standard relation between the two is revised. Some properties of the latter are also discussed, especially their manifestation in two-state systems, the central focus of this thesis. Following [12], the definitions are generalized to cope with mixed states, the listed properties analysed to find how do they change and some specific calculations relevant to two-state systems are done.

3.1 Pancharatnam's phase

Let us consider the following situation: a quantum state $|\psi\rangle$ undergoes some kind of cyclic evolution and ends in the state $e^{i\phi}|\psi\rangle$. The physical state is the same and the expectation value of any observable is the same for both states. However, if we had two copies of the initial state, we could make one of them undergo the evolution, compare it with the second copy (using interferometry, for instance) and extract the quantity ϕ. It then seems very natural to consider it as the "relative phase" between both states. Accordingly, the mathematical definition is given by (3.1).

$$\begin{aligned} |\psi_0\rangle &= |\psi\rangle \\ |\psi_f\rangle &= e^{i\phi}|\psi\rangle \\ \phi &= \arg\langle\psi_0|\psi_f\rangle \end{aligned} \tag{3.1}$$

This definition can be extended to cases in which the evolution is no longer cyclic. The final state is then no longer equal to the initial state multiplied by a phase factor but (3.1) is still a well defined quantity (except when both states are orthogonal)

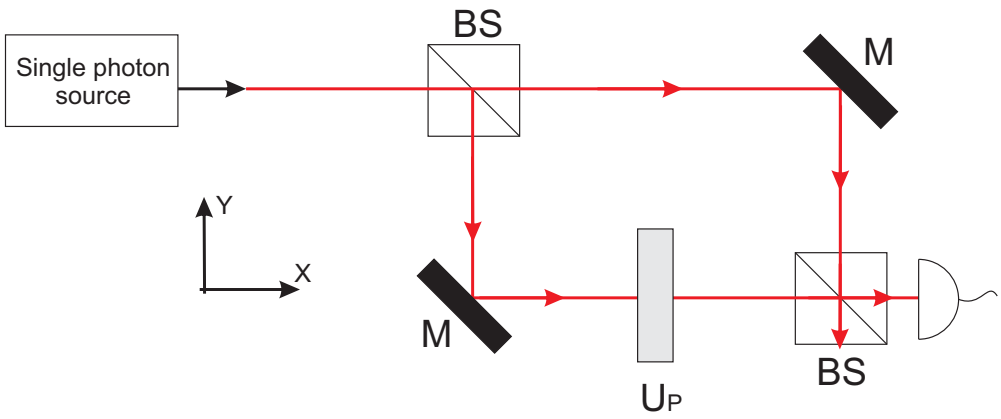

Figure 3.1: Optical array that introduces a Pancharatnam phase shift. The sequence of operations the photon undergoes is described in the text.

and is known as the Pancharatnam phase [13] between $|\psi_0\rangle$ and $|\psi_f\rangle$. This definition can also be experimentally motivated by considering the setup in Fig.(3.1). A horizontally polarized photon enters the first BS through input X. Its quantum state then undergoes a sequence of operations: the action of the first BS and the mirrors (3.2),

$$|H\rangle|X\rangle \rightarrow |H\rangle|X\rangle + |H\rangle|Y\rangle \tag{3.2}$$

a polarization transformation that acts only on one arm of the interferometer (3.3),

$$\rightarrow |H\rangle|X\rangle + |P_f\rangle|Y\rangle \tag{3.3}$$

the final BS (3.4),

$$\rightarrow (|H\rangle + |P_f\rangle)|X\rangle + (|H\rangle - |P_f\rangle)|Y\rangle \tag{3.4}$$

and a projection on the path degree of freedom (3.5). We have also included a possible phase difference originated by unequal arm lengths (φ) and have not normalized the states.

$$P_X \propto ||H\rangle + |P_f\rangle|^2 \propto 1 + |\langle H|P_f\rangle| \cos\left(\arg\langle H|P_f\rangle + \varphi\right) \tag{3.5}$$

If there were no polarization transformation (the map $|H\rangle \rightarrow |P_f\rangle$ in (3.3)) then the probability of detecting a photon in arm X would be $P_X \propto 1 + \cos\varphi$ and an interferogram could be constructed by varying φ. If the transformation is performed, the interferogram changes in the two very clear ways seen in Fig.(3.2): the visibility is reduced and a phase shift equal to the Pancharatnam phase appears. The Pancharatnam phase is, therefore, an experimentally measurable quantity.

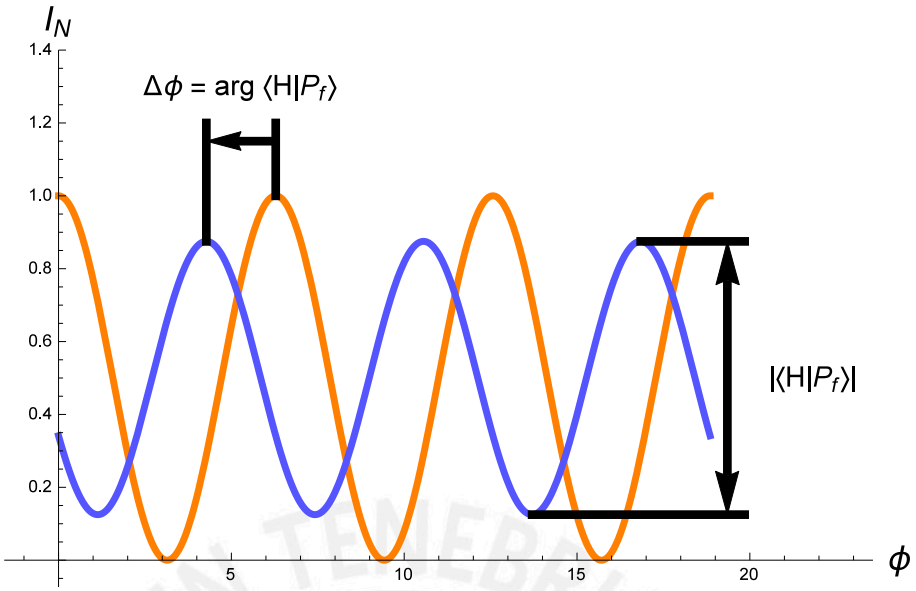

Figure 3.2: ϕ and I_N correspond to φ and P_X in Eq.(3.5). The orange curve is the standard interferogram that is measured when no polarization transformation is applied and path-length difference is varied. The blue curve is measured when a $U_P \neq 1$ is applied. The phase shift and change in visibility are manifest.

3.2 Geometric phase

From the theoretical side another phase was defined in 1984 by Michael Berry [1]. Though initially surprising because the main result contradicted the standard lore about the adiabatic approximation, the subject has grown quite a lot and the concepts have been generalized and applied to very different situations. First of all, many known phenomena have been interpreted in the light of this concept of geometric phase. The Foucault pendulum, motion in slightly non-uniform magnetic fields and the backreaction of the electron system on the heavy-ion system in metals [14] are some examples of them. There have also been numerous proposals to implement quantum logic gates based on geometric phases [2, 15, 16] because there are arguments showing its resilience to different kinds of noise that are expected to be present on any real implementation of a quantum computer. The literature is not conclusive in this respect [17], with some studies showing that it is more sensitive than other proposals to control parameter noise [18] and decoherence [19], while others reach the opposite conclusion [20]. Some experimental studies in this line are [6, 21] It has also been measured numerous times in different physical systems: superconducting circuits [3], ultracold neutrons [22], photon polarization [5], etc. In yet another experimental context, geometric phases are also used to fabricate artificial gauge fields [8], both Abelian and non-Abelian. Interest in a related cousin of

the geometric phase, one that is related to the topology of the space in which some kind of evolution occurs, has also arisen [23–25]. It has been found to be relevant in condensed matter systems such as topological insulators [7].

3.2.1 Berry's original approach

Even though most of the conditions imposed by Michael Berry to study geometric phases were later relaxed, it is instructive to describe and analyze the situation he originally considered [1] because it is much more directly connected to physical systems. We will first describe qualitatively the conclusions to which he arrived and then complement them with the appropriate mathematical treatment.

Consider a spin 1/2 system in the presence of a constant classical magnetic field. The solution to the spin's time development can be very easily stated: the spin vector (given by $\boldsymbol{s}(t) = \langle\psi(t)|\boldsymbol{\sigma}|\psi(t)\rangle$) precesses around the magnetic field at a constant rate, proportional to the magnitude of $\boldsymbol{B}$. What Berry did was to consider the situation in which the field's direction changed very slowly as compared to the precession period of the spin and in which both were initially aligned. As a result, the spin vector slowly followed the magnetic field throughout its movement in 3D space (see Fig.3.3a). In the final situation, after performing a closed loop, both $\boldsymbol{B}$ and $\boldsymbol{s}$ end up pointing in the initial direction (Fig.3.3b). Under this conditions, one can also calculate the evolution of the system's state vector. If it started in state $|\psi_0\rangle$, the final state can at most differ by a phase factor from the initial state ($|\psi_f\rangle = e^{i\phi}|\psi_0\rangle$) since the spin vector ends up pointing in the initial direction. Schrödinger's equation allows us to calculate ϕ explicitly, and what Berry found was that it could not be gauged away (we will shortly clarify what this means). This suggested that it must be somehow related to a property of the spin vector's trajectory (evolution in projection space), and he succeeded in proving that there was a contribution to ϕ called ϕ_G such that $\phi_G = -\Omega/2$, where Ω is the solid angle subtended by the curve traversed by the spin vector as it evolved under the action of $\boldsymbol{B}$.

By gauging away the phase we mean the following: given a magnetic field $\boldsymbol{B}$, a state vector that describes a spin pointing in the same direction as $\boldsymbol{B}$ is

$$|\boldsymbol{B}\rangle = \cos(\theta_{\boldsymbol{B}}/2)|\uparrow\rangle + \sin(\theta_{\boldsymbol{B}}/2)e^{i\xi_{\boldsymbol{B}}}|\downarrow\rangle \tag{3.6}$$

As the evolution develops, $\boldsymbol{B}$ becomes a function of time and so the system's state vector is given by $e^{i\phi(t)}|\boldsymbol{B}(t)\rangle$ where it is understood that $|\boldsymbol{B}\rangle$ is always of the form given by (3.6). When $\boldsymbol{B}$ closes a loop after time T, then $|\boldsymbol{B}(0)\rangle = |\boldsymbol{B}(T)\rangle$

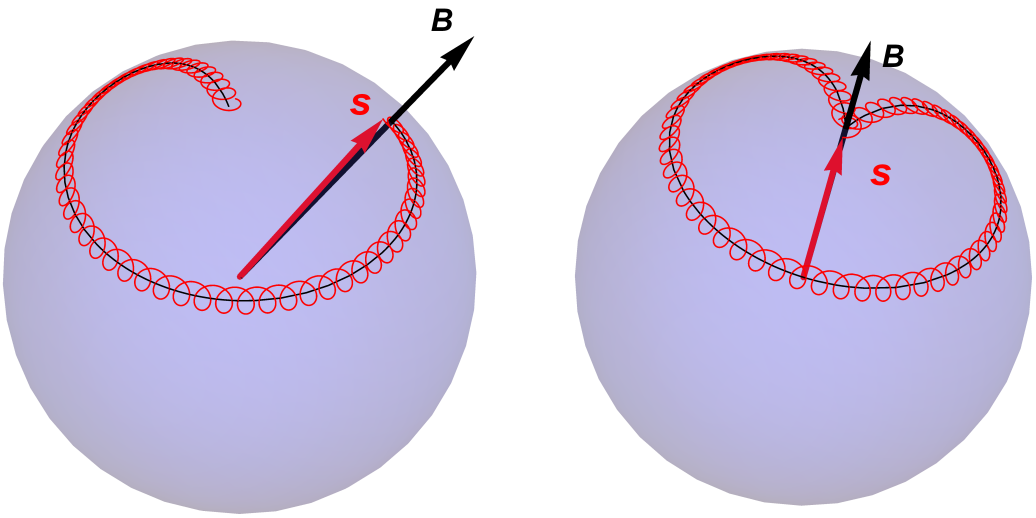

(a) (b)

Figure 3.3: Trajectories followed by the spin vector and magnetic field when the latter changes its direction adiabatically. The former precesses quickly about the instantaneous $\boldsymbol{B}$ as it evolves smoothly (if they are not initially aligned). (a) shows an open curve, while (b) shows that when $\boldsymbol{B}$ does a closed loop, so does $\boldsymbol{s}$ approximately.

because $|\boldsymbol{B}\rangle$ is a function of time only indirectly through $\boldsymbol{B}$ and $\boldsymbol{B}(0) = \boldsymbol{B}(T)$. One could redefine $|\boldsymbol{B}'\rangle = e^{i\alpha(\boldsymbol{B})}|\boldsymbol{B}\rangle$ trying to make $e^{i\phi(t)}$ disappear and it turns out one can do that for most times. This, however, does not work for $t = T$. Such a transformation is known as a gauge transformation and so, in this language, $\phi(T)$ cannot be "gauged" away. For comparison purposes, we reproduce the full calculation of $\phi(t)$ and show the gauge invariance of $\phi(T)$.

First of all, a general spin 1/2 state can be written as $|\psi\rangle = c_+(t)|\boldsymbol{B}(t)\rangle + c_-(t)|-\boldsymbol{B}(t)\rangle$. Plugging this into Schrödinger's equation and projecting into $\langle\boldsymbol{B}(t)|$ we obtain (3.7) by taking into account that $|\boldsymbol{B}(t)\rangle$ is the instantaneous eigenvector (with eigenvalue $E_{\boldsymbol{B}(t)}$) of the standard spin 1/2 Hamiltonian: $\hat{H} = -\mu\boldsymbol{\sigma}\cdot\boldsymbol{B}(t)$.

$$\begin{aligned}\langle\boldsymbol{B}(t)|i\frac{d}{dt}|\psi\rangle &= i\frac{dc_+(t)}{dt} + ic_+(t)\langle\boldsymbol{B}(t)|\frac{d}{dt}|\boldsymbol{B}(t)\rangle + ic_-(t)\langle\boldsymbol{B}(t)|\frac{d}{dt}|-\boldsymbol{B}(t)\rangle \\ \langle\boldsymbol{B}(t)|\hat{H}|\psi\rangle &= c_+E_{\boldsymbol{B}(t)}\end{aligned} \tag{3.7}$$

Adiabaticity guarantees us that $\langle\boldsymbol{B}(t)|\frac{d}{dt}|-\boldsymbol{B}(t)\rangle \approx 0$. This can be seen by taking the time derivative of $\boldsymbol{\sigma}\cdot\boldsymbol{B}|-\boldsymbol{B}(t)\rangle = -B(t)|-\boldsymbol{B}(t)\rangle$ (B is the magnitude of $\boldsymbol{B}$) and then projecting on $\langle\boldsymbol{B}(t)|$. The result is shown in (3.8), where $\boldsymbol{b}$ is the unit

vector directed along $\boldsymbol{B}$. By looking at (3.7) and noticing that the typical timescale of evolution is given by frequency $E/\hbar$, we see that if the direction of $\boldsymbol{B}$ changes slowly as compared to $E/\hbar$, then we can neglect the term we have analyzed.

$$\begin{aligned}\langle \boldsymbol{B}(t)|\frac{d}{dt}|-\boldsymbol{B}\,(t)\rangle &= -\frac{1}{2}\langle \boldsymbol{B}(t)|\,\boldsymbol{\sigma}\cdot\,\frac{1}{B}\frac{d\boldsymbol{B}}{dt}|-\boldsymbol{B}\,(t)\rangle \\ &= -\frac{1}{2}\langle \boldsymbol{B}(t)|\,\boldsymbol{\sigma}\cdot\,\frac{d\boldsymbol{b}}{dt}|-\boldsymbol{B}\,(t)\rangle \end{aligned} \tag{3.8}$$

Because of this, (3.7) reduces to (3.9) and can be exactly solved.

$$i\frac{dc_+(t)}{dt} + ic_+(t)\langle \boldsymbol{B}(t)|\frac{d}{dt}|\boldsymbol{B}(t)\rangle = c_+ E_{\boldsymbol{B}(t)} \tag{3.9}$$

Plugging in the initial conditions ($c_+(0)=1$, $c_-(0)=0$) we arrive at the conclusion that c_+ is a pure phase factor (3.10) and that $|\psi(t)\rangle = c_+(t)|\boldsymbol{B}(t)\rangle = e^{i\phi(t)}|\boldsymbol{B}(t)\rangle$, with $\phi(t)$ given by (3.11).

$$c_+(t) = e^{i(-\int_0^t E_{\boldsymbol{B}(t)}dt + i\int_0^t \langle \boldsymbol{B}(t)|\frac{d}{dt}|\boldsymbol{B}(t)\rangle dt)} \tag{3.10}$$

$$\phi(t) = -\int_0^t E_{\boldsymbol{B}(t)}dt + i\int_0^t \langle \boldsymbol{B}(t)|\frac{d}{dt}|\boldsymbol{B}(t)\rangle dt \tag{3.11}$$

Instead of using the set of $|\boldsymbol{B}\rangle$ kets we could have used the $|\boldsymbol{B}'\rangle = e^{i\alpha(\boldsymbol{B})}|\boldsymbol{B}\rangle$ kets. The solution of Schrödinger's equation did not rely on any of these specific gauges, so we can reexpress the final result as $|\psi(t)\rangle = e^{i\phi'(t)}|\boldsymbol{B}'(t)\rangle$ with ϕ' given by (3.12). Note that the eigenvalues of $\hat{H}$ are independent of gauge as well.

$$\phi'(t) = -\int_0^t E_{\boldsymbol{B}(t)}dt + i\int_0^t \langle \boldsymbol{B}'(t)|\frac{d}{dt}|\boldsymbol{B}'(t)\rangle dt \tag{3.12}$$

Gauging away the phase means that by choosing adequately the set of $|\boldsymbol{B}'\rangle$ we can make $\phi'(t)=0$. To do this explicitly we replace the definition of the $|\boldsymbol{B}'\rangle$ in terms of the $|\boldsymbol{B}\rangle$ in (3.12) and arrive at (3.13) and (3.14).

$$\begin{aligned}\langle \boldsymbol{B}'(t)|\frac{d}{dt}|\boldsymbol{B}'(t)\rangle &= \langle \boldsymbol{B}(t)|e^{-i\alpha(\boldsymbol{B}(t))}\frac{d}{dt}(e^{i\alpha(\boldsymbol{B}(t))}|\boldsymbol{B}(t)\rangle) \\ &= \langle \boldsymbol{B}(t)|\frac{d}{dt}|\boldsymbol{B}(t)\rangle + i\frac{d\alpha(\boldsymbol{B}(t))}{dt}\end{aligned} \tag{3.13}$$

$$\begin{aligned}\phi'(t) &= -\int_0^t E_{\boldsymbol{B}(t)}dt + i\int_0^t \langle \boldsymbol{B}(t)|\frac{d}{dt}|\boldsymbol{B}(t)\rangle dt - \int_0^t \frac{d\alpha(\boldsymbol{B}(t))}{dt}dt \\ \phi'(t) &= \phi(t) - (\alpha(\boldsymbol{B}(t)) - \alpha(\boldsymbol{B}(0)) = \phi(t) - \Delta\alpha\end{aligned} \tag{3.14}$$

It then seems very straightforward to nullify $\phi'(t)$ by adjusting $\Delta\alpha$. However, this cannot be done at $t = T$. The reason is that $\boldsymbol{B}$ returns to its initial position, and so $|\boldsymbol{B}'(T)\rangle = |\boldsymbol{B}'(0)\rangle$. This implies that $e^{i\alpha(\boldsymbol{B}(T))}|\boldsymbol{B}(T)\rangle = e^{i\alpha(\boldsymbol{B}(0))}|\boldsymbol{B}(0)\rangle$, and since $|\boldsymbol{B}(T)\rangle = |\boldsymbol{B}(0)\rangle$ as well, it follows that $\alpha(\boldsymbol{B}(T)) - \alpha(\boldsymbol{B}(0))$ must be an integer multiple of 2π. This leaves no freedom to cancel $\phi(T)$.

This property of gauge invariance (module 2π) is also shared by the quantity $\phi_G = i\int_0^T \langle \boldsymbol{B}(t)|\frac{d}{dt}|\boldsymbol{B}(t)\rangle dt$ which can be seen to be just a part of ϕ. It is quite obvious from its definition that it does not depend on the way $\boldsymbol{B}$ changes with time. As far as evaluation of the integral goes, time is just a parameter and the integral is seen to be reparametrization invariant (a feature that ϕ itself does not share, which is why the ϕ_G part has been singled out). The only important thing is the curve that the magnetic field performed as the evolution unfolded. This means that ϕ_G can be rewritten as (3.15), where Stokes' theorem has been used to transform the line into a surface integral in the space of parameters of the Hamiltonian ($\boldsymbol{B}$).

$$\phi_G = i\oint_C \langle \boldsymbol{B}|\boldsymbol{\nabla}_{\boldsymbol{B}}|\boldsymbol{B}\rangle \cdot d\boldsymbol{B} = \int_S \boldsymbol{\nabla}_{\boldsymbol{B}}\times(i\langle \boldsymbol{B}|\boldsymbol{\nabla}_{\boldsymbol{B}}|\boldsymbol{B}\rangle)\cdot d\boldsymbol{S} \tag{3.15}$$

Parametrizing the surface S with the polar ($\theta_{\boldsymbol{B}}$) and azimuthal ($\xi_{\boldsymbol{B}}$) angles that $\boldsymbol{B}$ makes with the coordinate axes and using (3.6), the surface integral reduces to (3.17) after some manipulations (3.16).

$$\begin{aligned}\boldsymbol{\nabla}_{\boldsymbol{B}}\times(i\langle \boldsymbol{B}|\boldsymbol{\nabla}_{\boldsymbol{B}}|\boldsymbol{B}\rangle) &= i\boldsymbol{\nabla}_{\boldsymbol{B}}(\langle \boldsymbol{B}|)\times\boldsymbol{\nabla}_{\boldsymbol{B}}(|\boldsymbol{B}\rangle)\\ &= i\nabla_{\boldsymbol{B}}(\sin(\theta_{\boldsymbol{B}}/2)e^{-i\xi_{\boldsymbol{B}}})\times\nabla_{\boldsymbol{B}}(\sin(\theta_{\boldsymbol{B}}/2)e^{i\xi_{\boldsymbol{B}}})\\ &= \sin(\theta_{\boldsymbol{B}}/2)\cos(\theta_{\boldsymbol{B}}/2)\nabla_{\boldsymbol{B}}\xi_{\boldsymbol{B}}\times\nabla_{\boldsymbol{B}}\theta_{\boldsymbol{B}}\\ &= -\frac{1}{2}\frac{\boldsymbol{B}}{B^3}\end{aligned} \tag{3.16}$$

$$\phi_G = \int_S \boldsymbol{\nabla}_{\boldsymbol{B}}\times(i\langle \boldsymbol{B}|\boldsymbol{\nabla}_{\boldsymbol{B}}|\boldsymbol{B}\rangle)\cdot d\boldsymbol{S} = -\frac{1}{2}\int_S \frac{\boldsymbol{B}}{B^3}\cdot d\boldsymbol{S} = -\frac{1}{2}\int_S d\Omega \tag{3.17}$$

$$\phi_G = -\frac{\Omega}{2} \tag{3.18}$$

This provides further evidence of the gauge invariant character of either ϕ or ϕ_G. The trajectory followed by the spin vector or the magnetic field in 3D space is independent of the gauge chosen ($\boldsymbol{s}(t) = \langle \boldsymbol{B}(t)|\boldsymbol{\sigma}|\boldsymbol{B}(t)\rangle = \langle \boldsymbol{B}'(t)|\boldsymbol{\sigma}|\boldsymbol{B}'(t)\rangle$) and so is Ω, since it is defined entirely in terms of this trajectory (see Fig.3.4).

Some final points to consider are the following: both $\boldsymbol{s}$ and $\boldsymbol{B}$ performed the same path since they were always aligned, so a valid question is whether ϕ_G should be defined in terms of the curve made by $\boldsymbol{B}$ or by $\boldsymbol{s}$. Insofar as the example of this

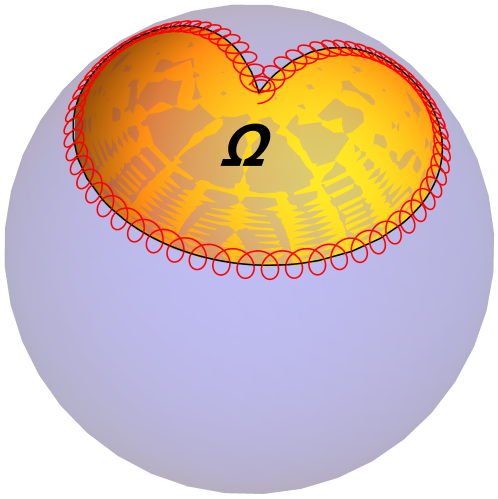

Figure 3.4: The relevant solid angle is shown when $\boldsymbol{B}$ does a closed loop. The geometric phase can be directly calculated from it.

section shows, the distinction is irrelevant. However, the difference turns out to have consequences in the non-adiabatic case since then $\boldsymbol{s}$ and $\boldsymbol{B}$ no longer remain aligned, even if they started so. The question of which of these trajectories should be considered becomes then a question about dynamics vs. kinematics because parameters such as $\boldsymbol{B}$ enter the evolution naturally through the Hamiltonian, whereas the trajectory made by $\boldsymbol{s}$ can be analyzed independently of the Hamiltonian that generated it.

3.2.2 Kinematic formulation

The discussion of the last section opens the question of how to generalize the definition of geometric phases so that more general situations can be encompassed. As developments of the field have shown, one can relax the conditions of adiabaticity, closed trajectories, use of pure states, unitary evolutions, etc. The price to pay is some degree of mathematical abstractness and some detachment from real physical systems. In any case, we will try to develop the exposition such that the concepts surveyed in the last section are connected to the definitions in this one so as to not loose the feeling of what we are talking about. We will follow the approach described in [26] and [27].

Definition

We will keep working with pure states and leave mixed states for later. Leaving that aside, the first question to be asked is what features are desirable in a more general

definition of geometric phases. Most of them are listed in the next paragraph.

1. It must reduce to Berry's result in the case of adiabatic cyclic evolution.

2. In two level-systems, it must depend on the path made by $\boldsymbol{s}$ rather than $\boldsymbol{B}$. The reason is one of simplicity. A general time varying $\boldsymbol{B}$ has a very complicated effect on the system. Relating in a simple way information about the curve made by $\boldsymbol{B}$ and some kind of phase in the system may prove to be very difficult.

3. In systems bigger than two-level, it must depend on the path made by $|\psi\rangle\langle\psi|$ (the system's density matrix) in projective space (P-space from now on). This is because in two-level systems, there is a one to one correspondence between $|\psi\rangle\langle\psi|$ and $\boldsymbol{s}$ ($|\psi\rangle\langle\psi| = \frac{1+\boldsymbol{s}\cdot\boldsymbol{\sigma}}{2}$). $|\psi\rangle\langle\psi|$ serves as a natural generalization of $\boldsymbol{s}$. This also ensures gauge invariance.

4. It must be independent of the parametrization of the curve made by $|\psi\rangle\langle\psi|$ since it must depend only on the curve itself.

A final remark is that, even if the geometric phase depends only on the curve in P-space, there is no inherent problem in defining it in terms of state vectors $|\psi\rangle$ as long as such a quantity possesses the properties that have been listed.
Building on the results of the previous section, a quantity invariant under curve re-parametrizations is (3.19).

$$i\int_0^t \langle \boldsymbol{B}(t)|\frac{d}{dt}|\boldsymbol{B}(t)\rangle dt \tag{3.19}$$

This suffers from various defficiencies, however. First of all, adopting the kinematic viewpoint means that reference to Hamiltonian parameters such as $\boldsymbol{B}$ must be avoided. Because of this, we consider the set of $|\psi(s)\rangle$ for $s \in [s_i, s_f]$ instead of $|\boldsymbol{B}(t)\rangle$. The set of $|\psi(s)\rangle$ defines a curve in Hilbert space (the succession of different $|\psi\rangle$ as s varies) and this curve has an image in P-space. With this prescription, (3.19) can be reformulated as (3.20).

$$-\phi_D = i\int_{s_i}^{s_f} \langle \psi(s)|\frac{d}{ds}|\psi(s)\rangle ds \tag{3.20}$$

(3.20) still suffers from a problem: it is not gauge invariant. Suppose we define $|\psi(s)\rangle = e^{-i\alpha(s)}|\psi'(s)\rangle$. In a way analogous to (3.14), we obtain:

$$-\phi_D = -\phi'_D + \alpha(s_f) - \alpha(s_i) \tag{3.21}$$

This time, however, there is no relation between $\alpha(s_f)$ and $\alpha(0)$ so they do not cancel each other. This illness can be cured by observing that the previously defined Pancharatnam phase (3.1) behaves in a very similar way under gauge transformations (3.24).

$$\phi_P = \arg\langle\psi(s_i)|\psi(s_f)\rangle \tag{3.22}$$
$$= \arg(\langle\psi'(s_i)|\psi'(s_f)\rangle e^{-i(\alpha(s_f)-\alpha(s_i))}) \tag{3.23}$$
$$= \phi'_P + \alpha(s_i) - \alpha(s_f) \tag{3.24}$$

This naturally implies that (3.25) is a gauge invariant quantity.

$$\phi_G = \arg\langle\psi(s_i)|\psi(s_f)\rangle + i\int_{s_i}^{s_f}\langle\psi(s)|\frac{d}{ds}|\psi(s)\rangle ds = \phi_P - \phi_D \tag{3.25}$$

The decomposition $\phi_G = \phi_P - \phi_D$ makes it clear that the Pancharatnam phase can be considered as the sum of two parts: a geometric one, that depends only on the geometry of the curve in P-space and a dynamic one that does not posses that property.

(3.25) will serve as the generalized definition of geometric phase. It has already been shown that it is both reparametrization and gauge invariant. It also reduces to the Berry phase in the situation he considered, as we argue next: when a system in an eigenstate of a nondegenerate $\hat{H}$ undergoes adiabatic evolution, its density matrix is in a one to one correspondence with the parameters of $\hat{H}$ for all times. Up to a gauge transformation, so are the state vectors. For definiteness, a gauge is chosen such that the state vector evolves only through its dependence on the Hamiltonian parameters. It is permissible to do so because any gauge will deliver the same answer. After a cyclic evolution, the Hamiltonian parameters return to their initial value, and so does the state vector. Because of this, the Pancharatnam phase after this trajectory is 0 (argument of 1). The geometric phase then reduces to expression (3.15).

Open and segmented curves

Definition (3.25) has some mathematical subtleties. Consider a curve in Hilbert space (and its image in P-space) composed of two segments: one goes from $|\psi_1\rangle$ to $|\psi_2\rangle$ and the second one from $|\psi_2\rangle$ to $|\psi_3\rangle$, as can be seen in Fig.(3.5). A valid question is how does the geometric phase of the whole (P-space) curve compares to the sum of the geometric phases of its segments. Since the dynamic phase is, by definition, an additive quantity, the difference is given entirely by the Pancharatnam

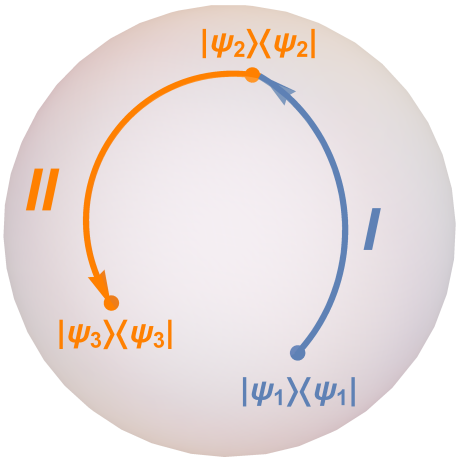

Figure 3.5: Two curves in P-space are shown. In the text it is argued that $\phi_G^{I+II} \neq \phi_G^I + \phi_G^{II}$. Thus, geometric phases are generally not additive functions of curves.

terms (3.26).

$$\phi_G^{I+II} - (\phi_G^I + \phi_G^{II}) = \arg(\langle\psi_1|\psi_3\rangle\langle\psi_3|\psi_2\rangle\langle\psi_2|\psi_1\rangle) \tag{3.26}$$

It is in general different from 0. When considering curves composed of more segments, the structure of expression (3.26) is preserved but longer chains of inner products appear.

Of particular interest is the case in which the full curve is closed in P-space and it is divided in just two segments, as in Fig.(3.6). Using (3.26) with $|\psi_3\rangle = e^{i\phi}|\psi_1\rangle$, the expression on the right hand side cancels because it reduces to $\arg(\langle\psi_1|\psi_2\rangle\langle\psi_2|\psi_1\rangle) = \arg(|\langle\psi_1|\psi_2\rangle|^2) = 0$. In this particular case the geometric phase is additive. This is a fact that will be important in the experimental section. From a theoretical point of view, such additiveness is also useful in assigning a geometric meaning to the geometric phase of an open curve. Let's start with curve I (see Fig.3.6), which is open in P-space. It can be closed with curve II, for which $\phi_G^{II} = 0$ (these curves do exist, as will be shown in a later section). Therefore $\phi_G^{I+II} = \phi_G^I$. The conclusion is that the geometric significance of ϕ_G^I is the same as the significance of the closed curve obtained by completing I with this special curve II. Thus, geometric significance of geometric phases of any kind of curve can be phrased in terms of closed curves and geometric phases in that context are more easily interpreted. In the Berry case, for example, they are related to solid angles.

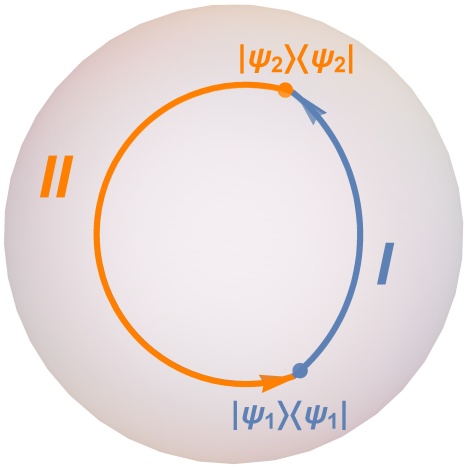

Figure 3.6: When two curves form a closed loop, their geometric phases are additive. See text for more details.

Zero geometric phase curves

Let's now consider these zero phase curves. We are only interested in the P-space curve. Therefore we are free to use any gauge we would like. In particular, we choose one such that the Pancharatnam phase becomes zero (this means $\langle\psi_0|\psi_f\rangle$ real and positive). The only remaining condition to guarantee zero geometric phase is (3.27)

$$\int_{s_0}^{s_f} \langle\psi(s)|\frac{d}{ds}|\psi(s)\rangle ds = 0 \tag{3.27}$$

This can be satisfied if the stronger condition $\langle\psi(s)|\frac{d}{ds}|\psi(s)\rangle = 0$ is enforced. Even then, it can be easily seen that the curve is not unique in general. To make this point clearer, let us restrict ourselves to a three-level system and work in an orthonormal basis in which the coefficients of $|\psi_0\rangle$ and $|\psi_f\rangle$ are all real. Both states can then be represented as points in the unit sphere in $\mathbb{R}^3$ (all states are normalized to unity). This can be done with any state that has real coefficients in this basis. It follows that a curve in this sphere represents a curve in Hilbert space that joins $|\psi_0\rangle$ and $|\psi_f\rangle$ only through states with real coefficients. The condition $\langle\psi(s)|\frac{d}{ds}|\psi(s)\rangle = 0$ is then automatically satisfied because in these kind of states it is equivalent to the normalization condition (a fact that can be easily verified by taking the derivative of $\langle\psi|\psi\rangle = 1$). Any such curve will accumulate no geometric phase.

The ambiguity in the definition of the zero phase curves means that the closed curve from which an open curve inherits its geometric significance is not unique. All these closed curves and the original open curve share the same geometric phase

and trying to relate it to some straightforward geometric quantity (such as solid angles) may prove to be complicated in general. In any case, it would be convenient to select among this closing curves one that possesses another geometric property. Fortunately the two-state system gives a clue as to what should this property be. It can be demonstrated that in this case the zero phase curve (in P-space) is unique and can be parametrized in the way shown by (3.28).

$$|\psi(s)\rangle = |\psi_0\rangle \cos(s) + (|\psi_f\rangle - |\psi_0\rangle \cos(s_f))\frac{\sin(s)}{\sin(s_f)} \qquad s \in [0, s_f]$$
$$\langle\psi_0|\psi_f\rangle = \cos(s_f) \tag{3.28}$$

Geodesics

Parametrization (3.28) makes no reference to the dimension of the Hilbert space involved, so it can be used in larger systems. In any case, the curve in P-space to which it is associated has an intriguing property. It minimizes a certain functional that is associated to the notion of distance in P-space. These curves are, therefore, geodesics and this is the property that will be required to unambiguously complete an open curve. They can be constructed by the following prescription [26].
The length element in $\mathbb{R}^N$ is identified with the expression $\frac{dl^2}{ds^2} = \sum_i \frac{dx_i}{ds}\frac{dx_i}{ds}$, where the x_i are the cartesian coordinates in the space. In an analogous manner, the coefficients of a state vector in a particular basis can be considered to be its coordinates in Hilbert space. With $|\psi\rangle = \sum_i c_i|i\rangle$, the line element would be $\frac{dl^2}{ds^2} = \sum_i \frac{dc_i^*}{ds}\frac{dc_i}{ds}$ where the complex conjugate has been included to guarantee that the expression is real and positive. Such an expression is in fact basis independent and can be rewritten as $\frac{dl^2}{ds^2} = \frac{d\langle\psi|}{ds}\frac{d|\psi\rangle}{ds}$. As it stands, it is gauge-dependent and so cannot represent any distance in P-space. This is because the quantity $\frac{d|\psi\rangle}{ds}$ does not transform in the same way as $|\psi\rangle$ (see 3.29).

$$|\psi'\rangle = e^{-i\alpha(s)}|\psi\rangle$$
$$\frac{d|\psi'\rangle}{ds} = e^{-i\alpha(s)}\left(\frac{d|\psi\rangle}{ds} - i\frac{d\alpha(s)}{ds}|\psi\rangle\right) \tag{3.29}$$

To fix it, some kind of covariant differentiation must be introduced in order that $(D|\psi\rangle)' = D'|\psi'\rangle = e^{-i\alpha(s)}D|\psi\rangle$. By examining (3.29), it becomes apparent that a change of gauge introduces a spurious longitudinal component (parallel to $|\psi\rangle$). This means that considering the component of $\frac{d|\psi\rangle}{ds}$ transverse to $|\psi\rangle$ might cure the problem. Defining $\frac{D|\psi\rangle}{ds} = \frac{d|\psi\rangle}{ds} - |\psi\rangle\langle\psi|\frac{d|\psi\rangle}{ds}$, a quick calculation shows that it satisfies $(D|\psi\rangle)' = e^{-i\alpha(s)}D|\psi\rangle$. Therefore $dl^2 = (D\langle\psi|)(D|\psi\rangle) = ||D|\psi\rangle||^2$ is

a gauge invariant quantity and can be used as a definition of distance in P-space. Geodesics are thus given by minimizing the funcional (3.30) subject to the restriction of constant magnitude of the state (3.31).

$$S = \int_0^{s_f} \sqrt{(D\langle\psi|)(D|\psi\rangle)} = \int_0^{s_f} \sqrt{\langle v|v\rangle - |\langle v|\psi\rangle|^2} ds \tag{3.30}$$

$$|v\rangle = \frac{d|\psi\rangle}{ds}$$

$$\langle\psi|\psi\rangle = 1 \tag{3.31}$$

Applying heuristically the calculus of variations to this problem (with a Lagrangian multiplier to enforce the constraint) results in equation (3.33).

$$L' = \sqrt{\langle v|v\rangle - |\langle v|\psi\rangle|^2} + \frac{1}{2}\lambda(s)\langle\psi|\psi\rangle \tag{3.32}$$

$$2\frac{d}{ds}\left(\frac{\partial L'}{\partial\langle v|}\right) = \frac{d}{ds}\left(\frac{|v\rangle - \langle\psi|v\rangle|\psi\rangle}{||D|\psi\rangle||}\right) = -\frac{\langle v|\psi\rangle|v\rangle}{||D|\psi\rangle||} + \lambda(s)|\psi\rangle = 2\frac{\partial L'}{\partial\langle\psi|} \tag{3.33}$$

Choosing a parametrization such that $||D|\psi\rangle|| = 1$ and a gauge in which $\langle\psi|v\rangle = 0$ (thus $|v\rangle = \frac{d|\psi\rangle}{ds} = D|\psi\rangle$) it becomes (3.34).

$$\frac{d}{ds}|v\rangle = \frac{d^2}{ds^2}|\psi\rangle = \lambda(s)|\psi\rangle \tag{3.34}$$

There is no problem with these choices since the only interest is the geodesic in P-space and this choice of gauge and parametrization amounts to selecting the most convenient representative curve in Hilbert space. By differentiating the gauge condition, $\lambda(s)$ can be determined (3.35).

$$\begin{aligned} 0 &= \frac{d}{ds}\langle\psi|v\rangle = (\frac{d}{ds}\langle\psi|)|v\rangle + \langle\psi|\frac{d}{ds}|v\rangle \\ &= \langle v|v\rangle + \langle\psi|\lambda(s)|\psi\rangle \\ 0 &= ||D|\psi\rangle||^2 + \lambda(s) = 1 + \lambda(s) \\ \lambda(s) &= -1 \end{aligned} \tag{3.35}$$

With this, (3.34) becomes (3.36).

$$\frac{d^2}{ds^2}|\psi\rangle = -|\psi\rangle \tag{3.36}$$

It is trivial to verify that the solution given by (3.28) satisfies (3.36), as well as $||D|\psi\rangle|| = 1$ and $\langle\psi|v\rangle = 0$. The procedure to construct the geodesic is then as

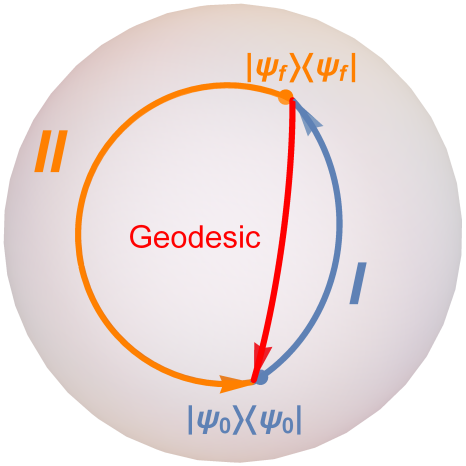

Figure 3.7: Same curves as in Fig.(3.6). This time, curve I is completed by a geodesic. The geometric phase of curve I equals that of curve I + geodesic, which is closed.

follows:

1. Given two points in projective space, $|\psi_0\rangle\langle\psi_0|$ and $|\psi_f\rangle\langle\psi_f|$, two representatives in Hilbert space are chosen: $|\psi_0\rangle$ and $|\psi'_f\rangle$ such that $\langle\psi_0|\psi'_f\rangle$ is real.

2. Those states are connected with the curve given by (3.28). The image of this curve in P-space is a geodesic and has zero geometric phase. See Fig.(3.7).

Two-dimensional case

After all this abstract detour we return to known territory and apply all these new concepts to the two-level system. First of all, if the curve followed by the system is closed (in P-space/Poincaré sphere), relation (3.37) holds.

$$\phi_G = -\frac{\Omega}{2} \tag{3.37}$$

If the curve is open, it can be closed by a geodesic and its geometric phase equals the one of the closed curve. Therefore, (3.37) is valid for the completed curve. The geometric phase of an open curve is minus one half the solid angle subtended by the curve when completed with a geodesic.

Let's examine more closely geodesics in this setting. Given two points in the Poincaré sphere, a basis (in Hilbert space) can always be selected such that $|\psi_0\rangle = |\psi_0\rangle$ and $|\psi_f\rangle = \cos(\theta)|\psi_0\rangle + \sin(\theta)|\psi_0^\perp\rangle$ with $|\psi_0\rangle$ and $|\psi_f\rangle$ being suitable Hilbert space representatives of the initial and final points in P-space and $\langle\psi_0|\psi_0^\perp\rangle = 0$. Plugging

this into (3.28) gives the curve $|\psi(s)\rangle = \cos(s)|\psi_0\rangle + \sin(s)|\psi_0^\perp\rangle$, $s \in [0, \theta]$. This shows that, in this case, the abstract notion of geodesic defined in the previous section is equivalent to the standard definition: it corresponds to a great circle, the shortest curve on the sphere.

To see this more clearly, consider $|\psi_0\rangle$ as a $|H\rangle$ state and $|\psi_0^\perp\rangle$ as a $|V\rangle$ state. Then, $|\psi_f\rangle$ is in the XY plane because it only has real coefficients (the X direction represents $|H\rangle$ and the Y direction represents $|D\rangle = \frac{|H\rangle+|V\rangle}{\sqrt{2}}$). By the same token, every $|\psi(s)\rangle$ is in the XY plane and thus, the curve is a great circle. The identification $|\psi_0\rangle \to |H\rangle$ and $|\psi_0^\perp\rangle \to |V\rangle$ amounts to a change of basis, which manifests itself as a rotation (and perhaps a reflection) in the Poincaré sphere. The property of being a great circle is not changed by these operations, so the curve connecting $|\psi_0\rangle\langle\psi_0|$ and $|\psi_f\rangle\langle\psi_f|$ is a great circle.

3.3 Extensions to mixed states

For the case of mixed states, two geometric phase definitions have been proposed and have been shown to be inequivalent: Sjökvist's [12] and Uhlmann's [28]. Even though it would be useful to make a parallel between both, in this thesis we will work only with the first one since it is the only one with which we have done the experiments. The following sections will motivate Sjökvist's definition, analyze its properties and compare them to the pure state case.

3.3.1 Sjövist's phase

Pancharatnam phase

The original setup that motivated the definition of Pancharatnam's phase (Fig.3.1) can be used to extend it to mixed states undergoing unitary evolution. The procedure is the following. Instead of an H polarized photon entering the interferometer, one can imagine its polarization state to be described by a density matrix ρ_P. Applying the sequence of operations outlined in section 1 results in the state transforming into (3.38).

$$T_X \rho_{Total} T_X \propto |X\rangle\langle X| \otimes (1 + e^{i\varphi} U_P)\rho_P(1 + e^{-i\varphi} U_P^\dagger) \tag{3.38}$$

In this opportunity the polarization transformation is represented by the unitary operator U_P instead of the mapping $|H\rangle \to |P_f\rangle$ described in the previous section because the initial state is no longer $|H\rangle$. However, both descriptions are equivalent if $\rho_P = |H\rangle\langle H|$ and $U_P|H\rangle = |P_f\rangle$. The T_X are projectors that project the state into the X output of the interferometer and φ is, once again, the phase difference between

the arms. The probability of detecting the photon in this arm can be extracted by tracing expression (3.38) obtaining thus a very simple formula (3.39) that is to be considered analogous to (3.5).

$$P_X \propto 1 + \Re(\mathrm{tr}(\rho_P U_P)e^{i\varphi}) = 1 + |\,\mathrm{tr}(\rho_P U_P)|\cos[\varphi + \arg(\mathrm{tr}(\rho_P U_P))] \tag{3.39}$$

As before, the interferogram obtained by varying φ is shifted with respect to the case in which $U_P = 1$ (the P subscripts will now be omitted). This phase shift is defined to be the Pancharatnam phase (3.40).

$$\phi_P = \arg(\mathrm{tr}(\rho U)) \tag{3.40}$$

It reduces to the previous result when $\rho = |H\rangle\langle H|$ and $U|H\rangle = |P_f\rangle$. In that case, $\mathrm{tr}(\rho U) = \mathrm{tr}(U|H\rangle\langle H|) = \mathrm{tr}(|P_f\rangle\langle H|) = \langle H|P_f\rangle \rightarrow \phi_P = \arg\langle H|P_f\rangle$. This definition can be understood as a weighted sum of phases. To see this, consider the quantity $\mathrm{tr}(\rho U)$ and express ρ in its eigenbasis with eigenvalues λ_i and eigenvectors $|\psi_i\rangle$ (3.41).

$$\mathrm{tr}(\rho U) = \sum_i \lambda_i \,\mathrm{tr}(|\psi_i\rangle\langle\psi_i|U) \tag{3.41}$$

The quantitites $\mathrm{tr}(|\psi_i\rangle\langle\psi_i|U) = \langle\psi_i|U|\psi_i\rangle$ can be written as $v_i e^{i\phi_{P,i}}$, where v_i and $\phi_{P,i}$ are the visibility and Pancharatnam phase shift of the interferogram that would have been obtained if the initial state had been $|\psi_i\rangle$ (as shown in (3.5)). Furthermore, $\mathrm{tr}(\rho U)$ can be expressed in the same way since $|\,\mathrm{tr}(\rho U)|$ and $\arg(\mathrm{tr}(\rho U))$ are the visibility and Pancharatnam phase shift of the interferogram that is being analyzed, as can be read from (3.39). Therefore, a relation between these various visibilities and phases can be established (3.42) and the Pancharatnam phase can be reexpressed as (3.43).

$$\mathrm{tr}(\rho U) = ve^{i\phi_P} = \sum_i \lambda_i v_i e^{i\phi_{P,i}} \tag{3.42}$$

$$\phi_P = \arg(\sum_i \lambda_i \langle\psi_i|U|\psi_i\rangle) \tag{3.43}$$

Geometric phase

(3.42) can be taken at face value and $\phi_{P,i}$ substituted directly by $\phi_{G,i}$ where, once again, $\phi_{G,i}$ is the geometric phase that would have been obtained if the initial state had been $|\psi_i\rangle$ (note that the $|\psi_i\rangle$ are pure states, so definition (3.25) can be directly applied). This relation will be used define what is meant by geometric phase of a mixed state, but before doing some things need to be stated clearly. Under the

action of U in (3.40), the kets $|\psi_i\rangle$ evolved into $|\psi_{i,f}\rangle = U|\psi_i\rangle$. The initial and final kets are all that matter for the Pancharatnam phase. On the other hand, geometric phases depend on the entire evolution that led into the state under consideration. Therefore, not only $|\psi_i\rangle$ and $|\psi_{i,f}\rangle$ matter, but all the $|\psi_i(s)\rangle$ in between (where s parameterizes the curve in Hilbert space under study). The curve followed by $|\psi_i(s)\rangle$ is the one that is used to calculate $\phi_{G,i}$ and since the latter is gauge invariant by construction, the complete mixed-state geometric phase ϕ_G is invariant under any gauge transformation of the kind $|\psi_i'(s)\rangle = e^{i\phi_i(s)}|\psi_i(s)\rangle$ for any i. Taking into account these considerations, definition (3.44) follows.

$$\begin{aligned} ve^{i\phi_G} &= \sum_i \lambda_i v_i e^{i\phi_{G,i}} \\ &= \sum_i \lambda_i v_i e^{i\phi_{P,i} - i\phi_{D,i}} = \sum_i \lambda_i \langle\psi_i|U|\psi_i\rangle) e^{-i\phi_{D,i}} \\ &= \sum_i \lambda_i \langle\psi_i|U|n_i\rangle e^{-\int_{\psi_i}^{s_f} \langle\psi_i(s)|\frac{d}{ds}|\psi_i(s)\rangle ds} \\ \phi_G &= \arg\Big(\sum_j \lambda_j \langle\psi_j(s_i)|\psi_j(s_f)\rangle e^{-\int_{s_i}^{s_f} \langle\psi_j(s)|\frac{d}{ds}|\psi_j(s)\rangle ds}\Big) \end{aligned} \tag{3.44}$$

In the pure state case, it reduces to (3.25) since then all the λ_i are zero except for one that is equal to one. This is shown in (3.45).

$$\begin{aligned} \phi_G &= \arg(\langle\psi(s_i)|\psi(s_f)\rangle e^{-\int_{s_i}^{s_f} \langle\psi(s)|\frac{d}{ds}|\psi(s)\rangle ds}) \\ &= \arg\langle\psi(s_i)|\psi(s_f)\rangle + \arg(e^{-\int_{s_i}^{s_f} \langle\psi(s)|\frac{d}{ds}|\psi(s)\rangle ds}) \\ &= \arg\langle\psi(s_i)|\psi(s_f)\rangle + i\int_{s_i}^{s_f} \langle\psi(s)|\frac{d}{ds}|\psi(s)\rangle ds \end{aligned} \tag{3.45}$$

What (3.44) tells is that to calculate the geometric phase of a mixed state undergoing a certain unitary evolution one must diagonalize ρ at each point in the evolution, find its eigenvalues (λ_i) and eigenvectors ($|\psi_i(s)\rangle$) and plug them into (3.44). It does not matter whether $|\psi_i(s)\rangle$ or $|\psi_i'(s)\rangle = e^{i\phi_i(s)}|\psi_i(s)\rangle$ are chosen as eigenvectors of $\rho(s)$, since the formula is invariant under that choice by construction.

Another way to think about (3.44) is the following. A curve with constant purity in the space of density matrices, $\rho(s)$ for $s \in [s_i, s_f]$, can be thought of as being generated by the action of some set of unitary operators acting on the initial state: $\rho(s) = U(s)\rho(s_i)U^\dagger(s)$. This does not define uniquely the $U(s)$, however. Indeed, for $\rho(s) = \sum_i \lambda_i |\psi_i(s)\rangle\langle\psi_i(s)|$, then $U(s)$ as well as $U'(s) = (\sum_i e^{i\phi_i(s)}|\psi_i(s)\rangle\langle\psi_i(s)|)U(s) = V(s)U(s)$ result in the same $\rho(s)$. The action of $V(s)$ is to map $|\psi_i(s)\rangle \to e^{i\phi(s)}|\psi_i(s)\rangle$ and thus implements gauge transformations on the eigenvectors of $\rho(s)$. There is an

infinite set of $V(s)$'s, one for each possible gauge transformation. What is remarkable is that whereas ϕ_P does differentiate between $U(s)$ and $U^{'}(s)$, ϕ_G is insensible to this choice. Any $U^{'}(s)$ that can be related to $U(s)$ by an operator of the form of $V(s)$ (which means that $U^{'}(s) = V(s)U(s)$ with $V(s)$ unitary and diagonal in the eigenbasis of $\rho(s)$) will give the same value for ϕ_G. This invariance under generic $V(s)$ is the statement of gauge invariance in this context and is demonstrated next.

$$\phi_G^{'} = \arg(\sum_j \lambda_j \langle\psi_j^{'}(s_i)|\psi_j^{'}(s_f)\rangle e^{-\int_{s_i}^{s_f}\langle\psi_j^{'}(s)|\frac{d}{ds}|\psi_j^{'}(s)\rangle ds})$$

$$\langle\psi_j^{'}(s_i)|\psi_j^{'}(s_f)\rangle = \langle\psi_j(s_i)|V^{\dagger}(s_i)V(s_f)|\psi_j(s_f)\rangle = \langle\psi_j(s_i)|\psi_j(s_f)\rangle e^{i(\phi_j(s_f)-\phi_j(s_i))}$$

$$\begin{aligned}
\int_{s_i}^{s_f}\langle\psi_j^{'}(s)|\frac{d}{ds}|\psi_j^{'}(s)\rangle ds &= \int_{s_i}^{s_f}\langle\psi_j(s)|V^{\dagger}(s)\frac{d}{ds}(V(s)|\psi_j(s)\rangle)ds \\
&= \int_{s_i}^{s_f}\langle\psi_j(s)|e^{-i\phi_j(s)}\frac{d}{ds}(e^{i\phi_j(s)}|\psi_j(s)\rangle)ds \\
&= \int_{s_i}^{s_f}\langle\psi_j(s)|e^{-i\phi_j(s)}\frac{d}{ds}(e^{i\phi_j(s)})|\psi_j(s)\rangle ds \\
&+ \int_{s_i}^{s_f}\langle\psi_j(s)|e^{-i\phi_j(s)}e^{i\phi_j(s)}\frac{d}{ds}|\psi_j(s)\rangle ds \\
&= \int_{s_i}^{s_f}\frac{d}{ds}(i\phi_j(s))ds + \int_{s_i}^{s_f}\langle\psi_j(s)|\frac{d}{ds}|\psi_j(s)\rangle ds \\
&= i(\phi_j(s_f)-\phi_j(s_i)) + \int_{s_i}^{s_f}\langle\psi_j(s)|\frac{d}{ds}|\psi_j(s)\rangle ds
\end{aligned}$$

$$\begin{aligned}
\phi_G^{'} &= \arg(\sum_j \lambda_j \langle\psi_j^{'}(s_i)|\psi_j^{'}(s_f)\rangle e^{-\int_{s_i}^{s_f}\langle\psi_j^{'}(s)|\frac{d}{ds}|\psi_j^{'}(s)\rangle ds}) \\
&= \arg(\sum_j \lambda_j \langle\psi_j(s_i)|\psi_j(s_f)\rangle e^{i(\phi_j(s_f)-\phi_j(s_i))} e^{-i(\phi_j(s_f)-\phi_j(s_i))-\int_{s_i}^{s_f}\langle\psi_j(s)|\frac{d}{ds}|\psi_j(s)\rangle ds}) \\
&= \arg(\sum_j \lambda_j \langle\psi_j(s_i)|\psi_j(s_f)\rangle e^{-\int_{s_i}^{s_f}\langle\psi_j(s)|\frac{d}{ds}|\psi_j(s)\rangle ds}) = \phi_G \\
\phi_G^{'} &= \phi_G
\end{aligned} \tag{3.46}$$

Two-state systems

In the case of two state systems, we can develop further the theory. As was shown previously, each density matrix can be mapped to a point in the volume within a unit sphere in three dimensions. Given an initial state $\rho = \frac{1}{2} + \frac{r}{2}\hat{\boldsymbol{n}} \cdot \boldsymbol{\sigma}$ $(0 \leq r \leq 1)$, $\hat{\boldsymbol{n}}$ indicates the direction of a vector in the Poincaré sphere and r is its length. The tip of the vector $r\hat{\boldsymbol{n}}$ represents ρ. A curve in the space of density matrices is then

identified with a curve in $\mathbb{R}^3$ within the sphere.

In the case of a closed curve ($\rho_f = \rho_i$) the curve is closed in $\mathbb{R}^3$ as well. Applying (3.44) with $|\langle\psi_j(s_i)|\psi_j(s_f)\rangle| = 1$ results in $\phi_G = \arg(\sum_j \lambda_j e^{i\phi_{G,i}})$. Now, $\phi_{G,j}$ is the geometric phase that the eigenstate $|\psi_j(s_i)\rangle$ of ρ would acquire under the evolution. It is equal to minus one half the solid angle subtended by the curve it traces as it evolves. Since the two orthogonal eigenstates of ρ are identified with antipode points in the Poincaré sphere, their geometric phases are equal in magnitude and of opposite sign (see Fig(3.8)). Furthermore, the solid angle associated to the eigenstate with the largest eigenvalue ($\lambda_j = \frac{1+r}{2}$) is equal to the solid angle associated to the curve traced out by the vector $r\hat{\boldsymbol{n}}$ which represents the original mixed state. Therefore, everything is naturally expressed in terms of this solid angle. With this provisos, the formula for the geometric phase (3.47) can then be modified into (3.48)

$$\phi_G = \arg(\sum_j \lambda_j e^{i\phi_{G,i}}) = \frac{1+r}{2}e^{-i\Omega/2} + \frac{1-r}{2}e^{i\Omega/2} \tag{3.47}$$

$$= \arg(\cos\frac{\Omega}{2} - ir\sin\frac{\Omega}{2})$$

$$\phi_G = \arctan(-r\tan\frac{\Omega}{2}) \tag{3.48}$$

(3.48) is clearly geometrical since it depends only on Ω and r.

Moving on to open curves, the first thing to study are geodesics. Since unitary evolution of a mixed state is constrained to a sphere of fixed radius r, standard geodesics are still great circles. It follows (through geometrical considerations) that if ρ traces a great circle, its eigenstates also trace great circles and thus acquire zero geometric phase. Applying the first line of (3.44) results in ϕ_G being the argument of a positive real number so it is zero. Mixed states undergoing geodesic evolution acquire no geometric phase. By the same token, when considering a general open curve, it is easier to analyze independently the eigenstates. If we complete the mixed state curve with a great circle (see Fig.(3.9)), the curve each eigenstate follows is also completed by a great circle. It does not contribute to their overall geometric phases (since the phase is additive for the eigenstates) and therefore they are equal to the phase of their open curves. In sum, the geometric phase of a curve (I) traced out by a state is equal to the phase of the curve that results from completing I with a great circle, even for mixed states (undergoing unitary evolution). Then (3.48) can be applied.

Nevertheless, some other properties of geometric phases are not retained. (3.26) showed that when a closed curve in P-space was divided in two, the sum of geometric phases of each part was equal to the geometric phase of the whole closed curve. This

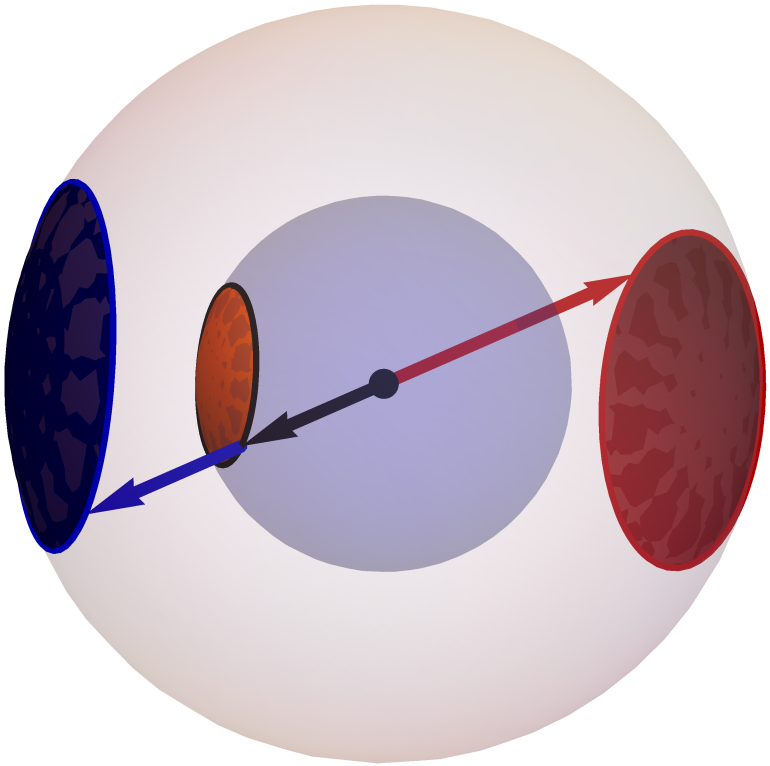

Figure 3.8: The black arrow represents the state $\rho = \frac{1+r}{2}|\hat{\boldsymbol{n}}\rangle\langle\hat{\boldsymbol{n}}| + \frac{1-r}{2}|-\hat{\boldsymbol{n}}\rangle\langle-\hat{\boldsymbol{n}}|$. The blue and red arrows represent the states $|\hat{\boldsymbol{n}}\rangle\langle\hat{\boldsymbol{n}}|$ and $|-\hat{\boldsymbol{n}}\rangle\langle-\hat{\boldsymbol{n}}|$ respectively. As ρ traces out the black curve, its eigencomponents trace out the blue and red curves. Because all shown surfaces enclose the same relative area (with respect to the area of sphere on which they lie), they subtend the same solid angle in magnitude. If the black curve is traversed in a counterclockwise fashion (with respect to the outward normal), so is the blue curve, but the red curve is done clockwisely. This accounts for the different signs in Eq.(3.47).

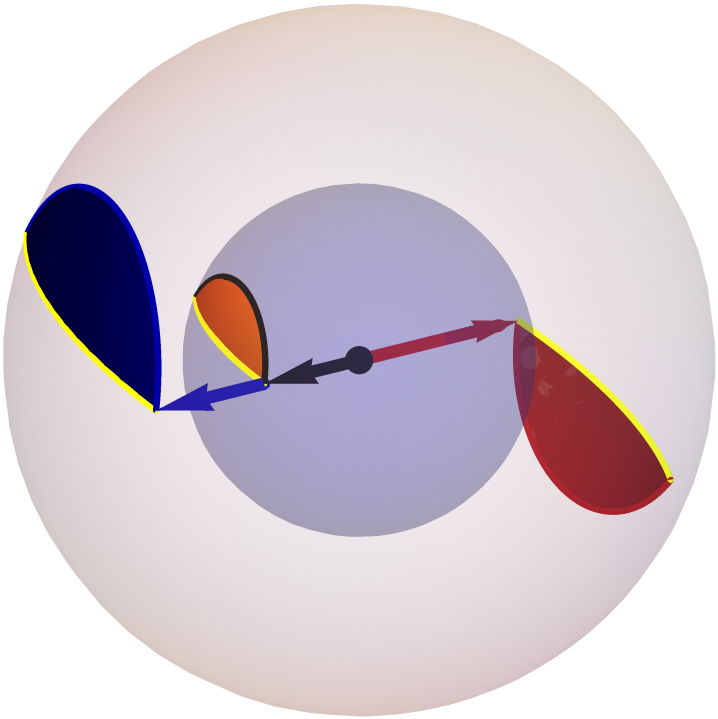

Figure 3.9: Same as for Fig.(3.8) but this time for open curves (black curve done by ρ). If the curve is completed by a geodesic (yellow curve), the curves followed by $|\hat{\boldsymbol{n}}\rangle\langle\hat{\boldsymbol{n}}|$ and $|-\hat{\boldsymbol{n}}\rangle\langle-\hat{\boldsymbol{n}}|$ are geodesics as well. Therefore, Eq.(3.48) can be directly applied using the solid angle subtended by the orange surface.

no longer holds generally (it does hold when one segment is a geodesic). As can be clearly seen, the additive quantities are the solid angles. Therefore (3.26) can be reformulated as (3.49).

$$\phi_G^{I+II} = \arctan[r \tan[\arctan(\frac{1}{r}\tan(\phi_G^I)) + \arctan(\frac{1}{r}\tan(\phi_G^{II}))]] \tag{3.49}$$

(3.49) is not neat, but will be useful to understand some features of the experiment.

Chapter 4

Experimental implementations

4.1 Mixed state generation

For quite some time there have been attempts to prepare partially polarized laser states, some of them with the objective of improving the calibration of polarimeters [29]. Things such as liquid-crystal displays [30–32] and interferometric setups [33] have been used. Part of the experiments reported in this thesis address this problem [34] in a way that does not require nor LCD's nor the stability needed for an interferometer. An identical solution was proposed afterwards by [35]. Furthermore, the array can be directly applied to the single-photon case furnishing a generator of arbitrary polarization mixed states. While such states have already been constructed, the studies focus on remote state preparation [36, 37] and generally on entangled states [38]. For the purposes of our experiments, an entangled photon source is not needed and would bring in unnecessary complications. More similar to our array is [39] but it was designed with the intent of implementing a pseudo-depolarizing channel rather than preparing arbitrary mixed states.

4.1.1 Laser source

The construction of a mixed state source in this context is tantamount to generating laser light with partial polarization. The language of pure and mixed states and density matrices, though designed to cope with quantum systems, can be applied to laser polarization in a way very similar to how polarization states of a single photon are handled. This was shown in chapter 2 and this paragraph is a reminder that one must be careful not to confuse the mathematical convenience of this correspondence with the physical nature of the systems under consideration. We refer the reader to chapter 2 to find a more detailed exposition in terms of quantum states.

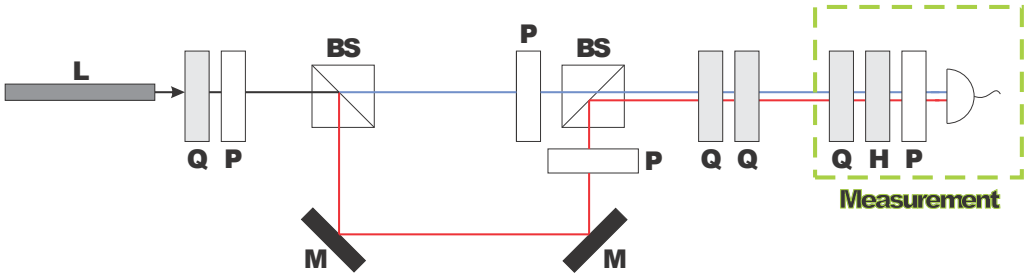

Figure 4.1: Polarization array. L: laser, BS: beam-splitter, M: mirror, Q: quarter-wave plate, H: half-wave plate, P: polarization filter, D: detector. The input state $|h\rangle$ is a horizontally polarized light-beam that is transformed into a state $\cos\theta\,|h\rangle + \sin\theta\,|v\rangle$ and then submitted to an array that first changes its degree of polarization and then its Stokes vector. The output state has the desired partial polarization, as can be confirmed at the measuring stage (enclosed part).

The guiding principle behind the partially polarized light source is the reduction of coherence between orthogonal polarizations. If this could be controlled at will, everything else follows, since transforming between different kinds of polarizations without changing coherence is straightforward (using wave plates). Since it is easier to work with linear polarizations, an array that controls coherence between horizontal and vertical components will be attempted.

The first way in which coherence could be reduced would be to somehow delay one of the components with respect to the other and take advantage of the finite coherence length of laser light. With sufficient delay, all coherence could be destroyed. This is unfeasible, though, because He-Ne lasers have a coherence length on the order of meters. To circumvent this problem, the array in Fig.(4.1) was developed.

Laser light with linear horizontal polarization enters the array and is transformed into light with linear polarization in the theta direction (4.1) using a polarizer.

$$|\theta\rangle = \cos\theta|H\rangle + \sin\theta|V\rangle \tag{4.1}$$

A quarter-wave plate (from now on denoted as Q) is set at 45° and placed before the polarizer to ensure that the light leaving the latter has a constant, θ-independent intensity.

Upon entering the first BS, light is divided equally in two arms and then enters two polarizers, one on each arm and set at 0° and 90°. This results in two beams with horizontal and vertical polarizations and intensities proportional to $\cos(\theta)^2$ and $\sin(\theta)^2$, respectively. They are once again recombined in a second BS such that

they do not overlap after leaving the array, but rather they propagate parallel to one another. A detector placed immediately after the BS would just sum their intensities and this guarantees the incoherence between both polarization components.
Ideally, the results of any measurement performed by the detector would be described by the polarization matrix shown in (4.2).

$$\rho = \cos(\theta)^2 |H\rangle\langle H| + \sin(\theta)^2 |V\rangle\langle V| \tag{4.2}$$

The logic behind it is very clear: it is just the incoherent sum of H and V polarizations with their respective intensities as weight. This can be seen even more clearly by referring to Eqs.(2.22) and (2.23) and noting that the contributions to ρ_{HH} and ρ_{VV} come from different regions of space, while there is no contribution to ρ_{HV} nor ρ_{VH} since there is no region of space that has an electric field with H and V components at the same time.
If the beams overlapped, the polarization states would sum coherently and a pure state would be obtained (with a different relative phase between components). Partial overlap would mean partial coherence and the array would not work as desired.
The degree of polarization can be controlled by changing the angle of the initial polarizer. This controls θ in (4.2) and therefore the relative weights of H and V polarization. In the Poincaré sphere, this means that any state in the X axis can be generated. We would like to generate any state on the sphere, however, not just on one axis. To achieve this, a unitary transformation is implemented with two wave plates at the output of the second BS (the two Q shown after the last BS in Fig.(4.1)). They perform the map $|H\rangle\langle H| \to |\hat{\boldsymbol{n}}\rangle\langle\hat{\boldsymbol{n}}|$ where $\hat{\boldsymbol{n}}$ denotes an arbitrary direction in the Poincaré sphere. Because of unitarity they also map $|V\rangle\langle V| \to |-\hat{\boldsymbol{n}}\rangle\langle-\hat{\boldsymbol{n}}|$. The final state is a generic polarization matrix (4.3), pointing in the direction $\hat{\boldsymbol{n}}$ (or $-\hat{\boldsymbol{n}}$ if $\cos(2\theta) \leq 0$) at a radius $|\cos(2\theta)|$.

$$\rho = \cos(\theta)^2 |\hat{\boldsymbol{n}}\rangle\langle\hat{\boldsymbol{n}}| + \sin(\theta)^2 |-\hat{\boldsymbol{n}}\rangle\langle-\hat{\boldsymbol{n}}| \tag{4.3}$$

Imperfections in the experiment are mostly due to different transmissions between both arms of the array (some elements may absorb and reflect more than others) and they are largely independent of θ. To model this, we insert a factor β, equal to the ratio between transmission coefficients, that multiplies the intensity of one of the arms. With this changes and after normalization, (4.3) is modified into (4.4).

$$\rho = \frac{\cos(\theta)^2 |\hat{\boldsymbol{n}}\rangle\langle\hat{\boldsymbol{n}}| + \beta \sin(\theta)^2 |-\hat{\boldsymbol{n}}\rangle\langle-\hat{\boldsymbol{n}}|}{\cos(\theta)^2 + \beta \sin(\theta)^2} \tag{4.4}$$

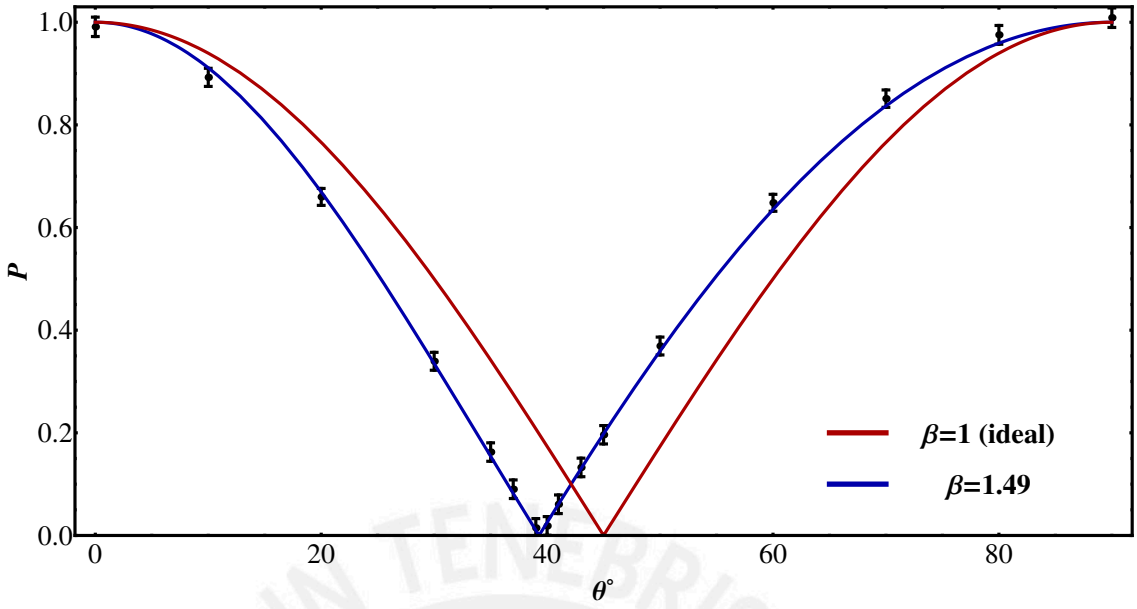

Figure 4.2: Degree of polarization of the laser source as a function of polarizer angle. The red curve corresponds to the ideal case ($\beta = 1$). All experimental departures from the ideal case are consistent with $\beta = 1.49 \pm 0.01$.

Even with this modification, the array is very convenient because the degree of polarization and the direction on the Poincaré sphere have independent controls. As can be seen, β is the only free parameter in the model. Therefore, the first experiment centered on its calibration. To achieve this, states with different θ were generated and their degree of polarization (P) was determined by measuring their Stokes parameters using the measurement stage shown in Fig.(4.1). A plot of P vs. θ is shown in Fig.(4.2), along with the ideal curve $P = |\cos(2\theta)|$ and the best-fit curve. The latter shows excellent agreement with the experimental results. The second experiment was designed to show that the array can generate almost any partially polarized state. A curve that explored many different regions of the Poincaré sphere was chosen and 28 points on it were generated (Fig.(4.3)). For each point on the curve, the previous calibration of β allowed the setting of the correct θ value in the first half-wave plate so that the targeted P was obtained. The last two wave plates were then adjusted to do the correct rotation in the Poincaré sphere (from the X axis, labelled as S1 in Fig.4.3, to the desired direction). To check that the targeted state was obtained, the Stokes parameters [11] were measured and the polarization state reconstructed (Fig.(4.4)).

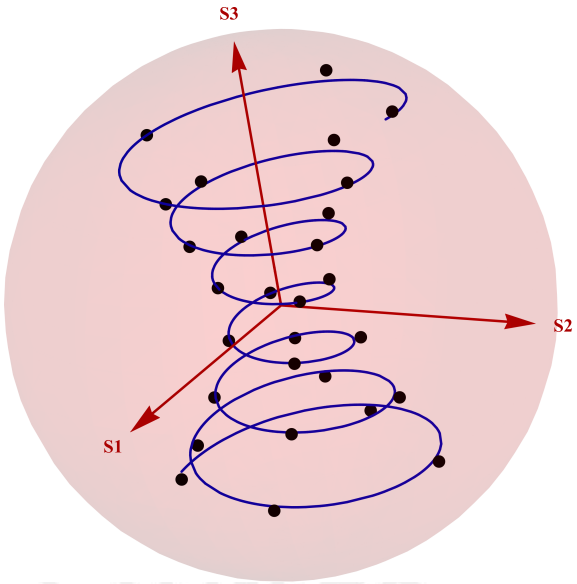

Figure 4.3: Trajectory followed within the Poincaré ball by varying both the degree of polarization and the Stokes vector of the laser source. The trajectory corresponds to the values plotted in Fig. (4.4).

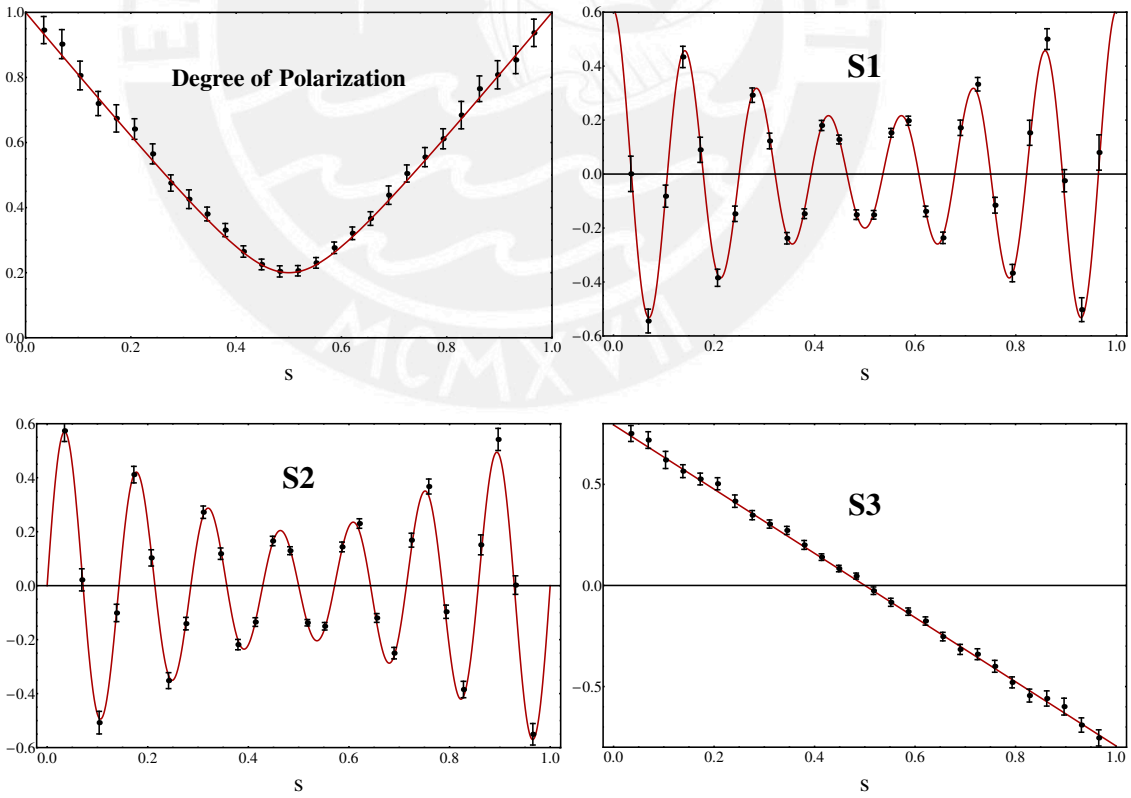

Figure 4.4: The degree of polarization and the three Stokes parameters of the laser light are shown as functions of the curve parameter.

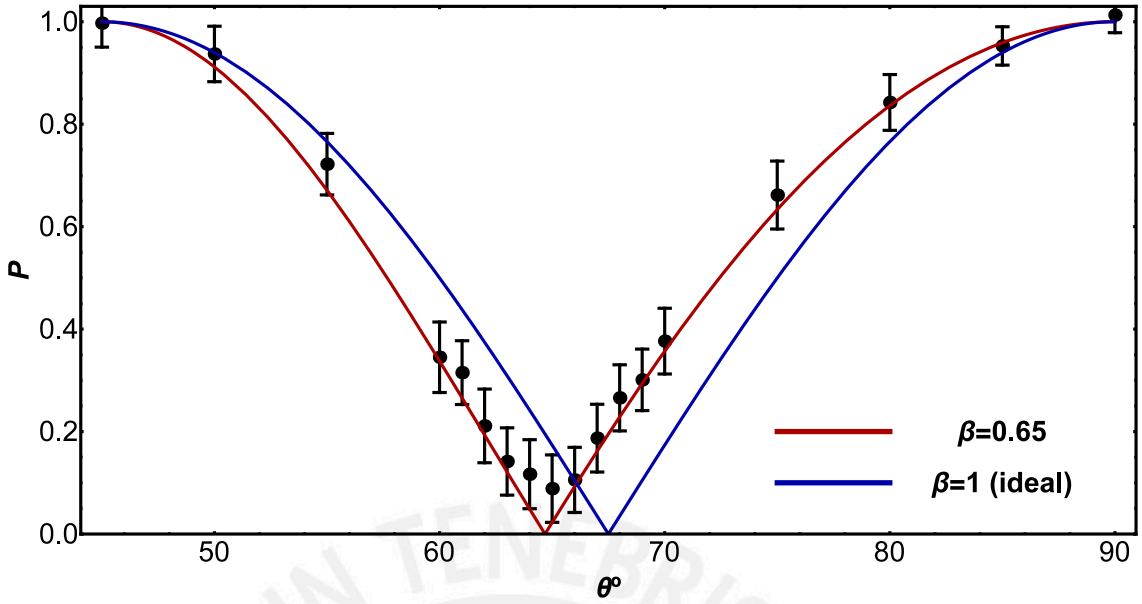

Figure 4.5: Degree of polarization of the single photon source as a function of polarizer angle. The red curve corresponds to the ideal case ($\beta = 1$). All experimental departures from the ideal case are consistent with $\beta = 0.65 \pm 0.01$.

4.1.2 Single photon source

In the case of the single photon source, the setup is almost the same as the one shown in Fig.(4.1). Because the path length difference between both arms of our array is on the order of centimeters while the photon coherence length is on the order of micrometers, single photon interference cannot be observed and both paths can be safely merged at the output of the last BS. They contribute incoherently and prepare a truly quantum mixed state. The experiments were done paralleling almost exactly those of the previous sections: a calibration procedure, shown in Fig.(4.5), that determines the value of β and the generation of mixed states that lie on a spiral curve within the Poincaré sphere, shown in Figs.(4.6) and (4.7). The graphs are completely analogous to the ones presented in section (4.1.1). Agreement is good once again, but errors are larger because a very dim single photon source with large statistical fluctuations was used. Furthermore, the experiments reported in this section were done with optical elements that were calibrated with a method that was later found out to be unreliable, in the sense that the method worked with some elements and not with others. Even though we cannot assert with certainty that those faulty elements were not used in this particular experiment, the lack of any systematic error makes us think that only correctly calibrated elements were employed.

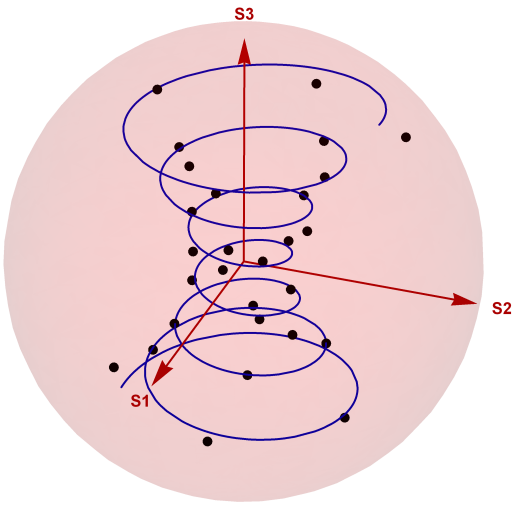

Figure 4.6: Trajectory followed within the Poincaré ball by varying both the degree of polarization and the Stokes vector of the single photon source. The trajectory corresponds to the values plotted in Fig. (4.7).

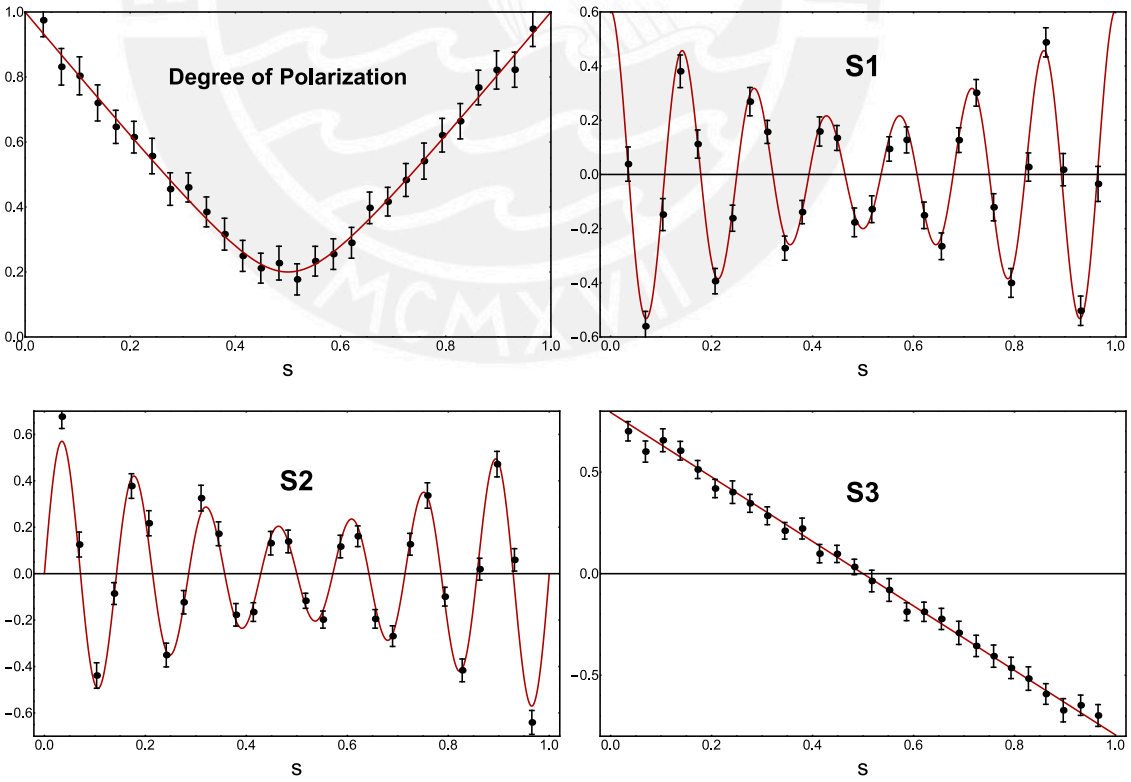

Figure 4.7: The degree of polarization and the three Stokes parameters of the single photon source are shown as functions of the curve parameter.

4.2 Geometric phase in mixed states

Measurements of mixed state geometric phases in two state systems have already been done [4,9]. However, they were restricted to very specific curves in the Poincaré sphere (closed and along great circles). The experiment presented in this section [40] deals instead with essentially arbitrary open curves.

4.2.1 Array and methodology

Discussion

To study geometric phases in mixed states, the first step is to generate the mixed state in question. Therefore, the array described in the previous sections is recycled and set as the first stage of a more complex experiment (prep stage in Fig.(4.9)). The preparation of the state is straightforward but the generation and measurement of geometric phases requires some more discussion and the following points need to be addressed:

1. Only means to measure the Pancharatnam phase have been provided, not the geometric phase.

2. The setup that motivated the definition of Pancharatnam phase involved an interferometer. This is highly inconvenient since the Mach-Zender array shown in Fig.(3.1), which is ideally suited to implement the experiment, is very unstable. One could use the more stable Sagnac interferometer, but this one suffers from a geometric impediment: the polarization transformation U_P must act only on one of the arms, not on both and this constraint is difficult to implement experimentally .

3. The only optical elements at hand (Q and H wave plates) perform a very restricted class of transformations in polarization space. Although one can transform one point in the Poincaré sphere into any other one, this cannot be done along an arbitrary route (unless the number of optical elements available is infinite).

Point 1 can be solved using the property of gauge invariance described in section 3.3.1. Given the trajectory in the Poincaré sphere whose geometric phase will be measured, it was shown that for each point in the evolution (s) there was an infinite set of unitaries $U'(s)$ that mapped the initial state ($\rho(s_i)$) to the state at that point ($\rho(s)$). The Pancharatnam phase developed by the system depended on which of these unitaries acted, but the geometric phase was the same for all of them. In

particular, there is a unitary $U_{||}(s)$ such that $\phi_G = \phi_P$. Therefore, among all the unitaries that cause the state to follow the trajectory in question, this special $U_{||}(s)$ is the one that should be implemented in the array of Fig.(3.1). It can be constructed from a generic $U(s)$ with the addition of an appropriate $V(s)$: $U_{||}(s) = V(s)U(s)$ in the sense of (3.46)

To circumvent the problems of interferometry described in point 2, a procedure devised by [41] was employed. The central point was to abandon the use of a real interferometer that operates on two degrees of freedom (photon polarization and momentum) and simulate a process of "virtual interferometry" using only polarization. The logic behind it is the following:

- A polarization state, such as $|H\rangle$, is interpreted as a state of momentum entering one of the ports of the first BS of an interferometer (while $|V\rangle$ would correspond to the other port).
- The polarization map $|H\rangle \rightarrow \frac{1}{\sqrt{2}}(|H\rangle + |V\rangle)$ is implemented because it simulates the action of a BS.
- Polarization states regain their interpretation as polarization states and the polarization transformation U_P is applied.
- Polarization states mimic momentum states again and the map $|H\rangle \rightarrow |H\rangle$, $|V\rangle \rightarrow e^{i\phi}|V\rangle$ is performed. This introduces a controllable "phase shift" that simulates the effects of arm length difference.
- The BS map is applied again.
- The state is projected into the ($|H\rangle$, $|V\rangle$) basis because this simulates the measurement of one of the outputs of the interferometer (detection in "arm $|H\rangle$ or in "arm $|V\rangle$").

The only modification needed to take into account an input state of the form $\rho = \lambda_1|\hat{\boldsymbol{n}}\rangle\langle\hat{\boldsymbol{n}}| + \lambda_2|-\hat{\boldsymbol{n}}\rangle\langle-\hat{\boldsymbol{n}}|$ rather than $|H\rangle$ is to modify the BS map into $|\hat{\boldsymbol{n}}\rangle \rightarrow \frac{1}{\sqrt{2}}(|\hat{\boldsymbol{n}}\rangle + |-\hat{\boldsymbol{n}}\rangle)$, the phase shift map into $|\hat{\boldsymbol{n}}\rangle \rightarrow |\hat{\boldsymbol{n}}\rangle$, $|-\hat{\boldsymbol{n}}\rangle \rightarrow e^{i\phi}|-\hat{\boldsymbol{n}}\rangle$ and to do the final projection in the $(|\hat{\boldsymbol{n}}\rangle, |-\hat{\boldsymbol{n}}\rangle)$ basis. The complete transformation is written in (4.5).

$$U_{int}(\phi) = U_{BS}U_{phase}(\phi)U_P U_{BS} \tag{4.5}$$

(4.5) has the inconvenience that $P(\phi) = \langle\hat{\boldsymbol{n}}|U_{int}(\phi)\rho_0 U_{int}^{\dagger}(\phi)|\hat{\boldsymbol{n}}\rangle$ (which includes the projection into "one arm of the interferometer") is a very nasty function of ϕ. This is, naturally, due to the fact that U_P does not commute either with U_{BS} or U_{phase},

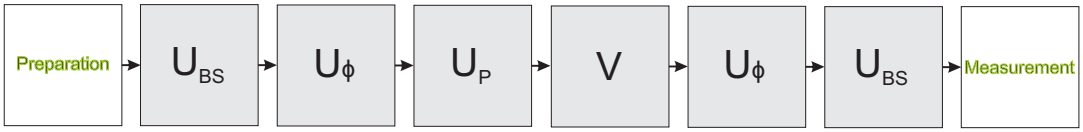

Figure 4.8: All the stages that the all-polarimetric setup must implement. At least 22 wave plates are needed.

a feature that the array in Fig.(3.1) does possess. This can be fixed by redefining $U_{int}(\phi)$ as shown in (4.6).

$$U_{int}(\phi) = U_{BS}U_{phase}(\phi)U_P U^{\dagger}_{phase}(\phi)U_{BS} \tag{4.6}$$

(4.6) has the advantage that then $P(\phi)$ is a sinusoidal function of ϕ (see Eq.(4.8)), making the correspondence with interferometry more tight. It will later be shown that in this setup, unlike interferometry, the Pancharatnam phase information is encoded in the visibility of the interferogram and not on the phase shift.
Finally, point 3 just means that a given trajectory in the Poincaré sphere cannot be done in one shot. Say one wants to measure the geometric phase as a function of the distance along the curve. What cannot be done is to devise a single evolution that makes the state follow the trajectory of interest as time passes and such that the Pancharatnam phase at each point is equal to the geometric phase acquired. For each point on the curve (s_1 for example), what can be done is to implement a unitary transformation (made up from optical elements) that maps $\rho(s_i)$ into $\rho(s_1)$ and such that the Pancharatnam phase is equal to the geometric phase that would have been obtained if the state had evolved along the curve under study. Note that it does not matter how does the system got from $\rho(s_i)$ to $\rho(s_1)$. This same process would be repeated for several points on the curve as the distance along it increases and a plot of geometric phase versus distance could be constructed.

Experimental array

Taking into account all that has been described, the experiment should follow the sequence shown in Fig.(4.8). There is a preparation stage, a U_{BS} stage, a U_{phase} stage, a U stage (made from a specific $U_P(s)$ plus the correction $V(s)$), another U_{phase} stage, another U_{BS} stage and a measurement stage. Except for the first and the last, they involve only wave plates and phase shifters. Now, it is widely known that any polarization SU(2) transformation can be implemented just with an array of three wave plates set at appropriate angles in the configuration QHQ [42]. Therefore, each of these stages must be at least a QHQ set (remember that both the

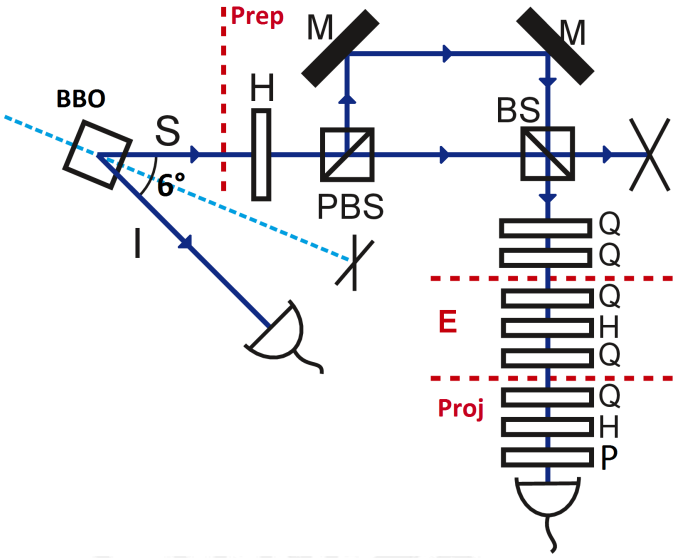

Figure 4.9: Experimental setup. In the preparation stage (Prep) the degree of polarization of single photons – generated by parametric down-conversion – is fixed by incoherently mixing $|H\rangle$ and $|V\rangle$ polarization states, after which the Stokes vector is brought to its desired orientation with the help of two quarter-wave plates. The next stage (E) consists of a QHQ array that implements the required unitary transformation (see text). The projection stage (Proj) serves to normalize coincidence counts (in the $|\mathbf{n}_{\pm}\rangle$ basis) between idler (I) and signal (S) photons.

BS and the phase transformation are diagonal in the same basis as the input stage, which is rather general). This means that at least 18 plates are needed. Summed to preparation (2 plates) and measurement (2 plates), the total rises to 22. While such an array allows the independent manipulation of each stage, it is very technically demanding and a large amount of error can be introduced.

Luckily, this can be simplified since the whole transformation (leaving preparation and measurement aside) is SU(2) in polarization. Thus, it can be replaced by an equivalent QHQ set and the total number of plates is reduced to 7. In principle, this could be applied to the other stages, but then preparation, evolution and measurement would be scrambled together, making any interpretation of the results very hard-pushed. On the other hand, this means that there is no independent control of the BS, phase and U_P transformations. Whenever one of those changes, the whole equivalent QHQ set must be prepared in a different configuration of angles. The resulting array is shown in Fig.(4.9).

The projection stage needs to be explained. As described before, the final action of an interferometer is a projection into one of its arms. In this "virtual interferometry" context, this means projecting into $|\hat{\boldsymbol{n}}\rangle$ or $|-\hat{\boldsymbol{n}}\rangle$. To do this operation, the QHP set shown in Fig.(4.9) was employed. The QH configuration transforms

the projector $|\hat{\boldsymbol{n}}\rangle\langle\hat{\boldsymbol{n}}|$ into $|H\rangle\langle H|$. As a consequence, setting the polarizer in the horizontal direction means that the whole QHP set projects the state into $|\hat{\boldsymbol{n}}\rangle\langle\hat{\boldsymbol{n}}|$. A slight modification allows the projection into $|-\hat{\boldsymbol{n}}\rangle\langle-\hat{\boldsymbol{n}}|$ as well.

Methodology

The experiment is structured in the following way. A (rather arbitrary) curve in the Poincaré sphere is chosen. The initial point determines the state that must be prepared ($\rho(s_i)$). This also fixes U_{BS}, the basis in which $U_{phase}(\phi)$ is diagonal and the projection basis. The only freedom left in $U_{phase}(\phi)$ is the phase ϕ. Then, a point in the curve, labelled by s', is chosen and this determines the state $\rho(s')$. One of the unitaries that maps $\rho(s_i)$ to $\rho(s')$ is chosen and with it, $U_{||}$ is calculated. U_P is then determined by setting it equal to $U_{||}$. Finally a phase ϕ^* is chosen and this fixes completely the array. Now that everything is known, the $U_{BS}U_{phase}(\phi^*)U_PU^\dagger_{phase}(\phi^*)U_{BS}$ part is replaced by its equivalent QHQ set. This changes nothing, since they implement the same transformation. Therefore, the probability of detecting the photon in the $|\hat{\boldsymbol{n}}\rangle$ state is still given by (4.7).

$$\begin{aligned} U_{int} &= U_{BS}U_{phase}(\phi^*)U_PU^\dagger_{phase}(\phi^*)U_{BS} \\ P(\phi^*) &= \langle\hat{\boldsymbol{n}}|U_{int}\rho(s_i)U^\dagger_{int}|\hat{\boldsymbol{n}}\rangle \end{aligned} \tag{4.7}$$

This can be calculated explicitly by expressing U_P in the form $U_P = e^{-i\alpha\hat{\boldsymbol{q}}\cdot\boldsymbol{\sigma}}$ that describes a rotation about the axis $\hat{\boldsymbol{q}}$ in the Poincaré sphere by an angle 2α. After a somewhat lengthy calculation (see Appendix A for details), (4.8) is obtained.

$$P = \frac{1+r}{2}\cos(\alpha)^2 + \frac{1-r\cos(\theta)^2}{2}\sin(\alpha)^2 + \frac{r}{2}\sin(\alpha)^2\sin(\theta)^2\cos(2\phi^* - 2\varphi) \tag{4.8}$$

θ is the angle that the vectors $\hat{\boldsymbol{n}}$ and $\hat{\boldsymbol{q}}$ make ($\theta = \arccos(\hat{\boldsymbol{n}}\cdot\hat{\boldsymbol{q}})$) and φ is an angle related to the choice of phase of $|-\hat{\boldsymbol{n}}\rangle$. Since the latter is inside the argument of the cosine, it just contributes a constant phase offset which won't affect the calculations. By repeating the process with different ϕ^* and leaving everything else untouched, an interferogram can be constructed and the minimum and maximum probabilities extracted (4.9).

$$\begin{aligned} P_{min} &= \frac{1-r}{2} + r\cos(\alpha)^2 \\ P_{max} &= \frac{1+r}{2} - r\cos(\theta)^2\sin(\alpha)^2 \end{aligned} \tag{4.9}$$

On the other hand, the Pancharatnam phase of the state $\rho(s_i)$ undergoing the evolution U_P is given by (4.10).

$$\begin{aligned}\phi_P &= \arg \mathrm{tr}(\rho(s_i)U_P) \\ &= \arg \mathrm{tr}[(\frac{1}{2} + \frac{r\hat{\boldsymbol{n}}\cdot\boldsymbol{\sigma}}{2})(\cos(\alpha) - i\hat{\boldsymbol{q}}\cdot\boldsymbol{\sigma}\sin(\alpha))] \\ &= \arg(\cos(\alpha) - ir\sin(\alpha)\hat{\boldsymbol{n}}\cdot\hat{\boldsymbol{q}}) \\ &= \arg(\cos(\alpha) - ir\sin(\alpha)\cos(\theta)) \\ \phi_P(\mathrm{mod}\pi) &= \begin{cases} -\arctan(r\tan(\alpha)\cos(\theta)), & \alpha < \pi/2 \\ \arctan(r\tan(\alpha)\cos(\theta)) - \pi, & \pi/2 < \alpha < \pi \end{cases}\end{aligned} \tag{4.10}$$

ϕ_P can be solved in terms of P_{max}, P_{min} and r. Furthermore, because of the special U_P chosen ($U_P = U_{||}$), this Pancharatnam phase is equal to the geometric phase that would have been obtained if the state had evolved along the chosen curve from $\rho(s_i)$ to $\rho(s')$. Thus, the geometric phase can be calculated in terms of explicitly measurable quantities (4.11).

$$\phi_G(\mathrm{mod}\pi) = \begin{cases} -\arctan(r\sqrt{\frac{1+r-2P_{max}}{2P_{min}-1+r}}) \\ \arctan(r\sqrt{\frac{1+r-2P_{max}}{2P_{min}-1+r}}) - \pi \end{cases} \tag{4.11}$$

Which of both should be used will be clarified shortly. All that has been said until now corresponds to just one point in the curve, $\rho(s')$. By repeating the procedure for different points, a curve of ϕ_G vs. s can be constructed. The requirement of continuity of this curve determines which of the formulas in (4.11) should be employed (starting from $\phi_G = 0$ for the initial point). As a side note, notice that for $s' = s_i$ ($\alpha = 0$), $P(\phi) = \frac{1+r}{2}$. This provides a convenient way of determining r experimentally.

The complete procedure can be described succinctly as follows:

1. Choose a curve in the Poincaré sphere beginning in an arbitrary initial state, $\rho(s_i)$.
2. Calculate U_{BS} and the configuration of the QHP plates in the measurement stage using $\rho(s_i)$.
3. Choose another point on the curve, $\rho(s')$.
4. Using $\rho(s_i)$, $\rho(s')$ and the chosen curve, calculate $U_{||}$.
5. Choose a phase ϕ^* and calculate $U_{phase}(\phi^*)$.

6. Calculate $U_{BS}U_{phase}(\phi^*)U_P U^{\dagger}_{phase}(\phi^*)U_{BS}$ and its QHQ equivalent.

7. Prepare the state $\rho(s_i)$, let it evolve in the QHQ evolution stage, project it with the QHP array and measure the probability of detection.

8. Construct the interferogram $P(\phi)$ vs. ϕ by repeating steps 5-7 varying ϕ.

9. Extract P_{max}, P_{min} and calculate $\phi_G(s')$ using (4.11) and the value of r given by the interferogram measured for $s' = s_i$.

10. Repeat steps 3-9 with a different s' and construct $\phi_G(s)$ vs. s.

4.2.2 Measurements

Technical information

Our single photon source is a barium borate crystal (BBO) which produces pairs of twin photons (810nm) by type-I spontaneous parametric downconversion. The crystal is pumped by 405nm cw diode laser (spectral linewidth between 0.5 and 1 nm and output power of 37.5 mW). The paths of the travelling photons make 3° each with the pump beam and 6° between them. The idler photon is sent directly into an avalanche photodetector, while the signal photon enters the preparation stage of the experiment. Coincidence counts of signal and idler beams are defined within a 10.42 ns time window. The photon-counting module (Perkin-Elmer SPCM-AQ4C) has a dark count rate of 500 ± 10 counts. Converging lenses are used to focus and couple them into multi-mode fiber-optic cables. Dichroic filters (Thorlabs FB800-40, FWHM:40 ± 8 nm) centered at 800 ± 8 nm are placed in front of the detector to avoid spurious counts. The degree of second-order coherence $g^{(2)}$ was measured between the reflected (R) and transmitted (T) beams of a beam splitter to check single-photon production. To do this, detections at gates T and R were made conditioned upon detection at a third gate (G). In this situation, $g^{(2)} = N_{GTR}N_G/(N_{GT}N_{GR})$, where N_k denote simultaneous photodetection at the gates labelled by k. In our case $g^{(2)} = 0.187 \pm 0.011$ was measured certifying that we are working with nonclassical light (requires $g^{(2)} < 1$).

The experiment made use of several zero-order quarter and half wave plates (Thorlabs WPQ05M-808 and WPH05M-808) designed for 808 nm mounted on Thorlabs RSP1/M rotation mounts, a Glan-Thomson polarizer (Thorlabs GTH5M-B), a Thorlabs BS-017 beam splitter and a Thorlabs PBS-252 polarizing beam splitter. The rotation mounts allowed for a ±1° precision in waveplate angle setting.

Experimental details

Three curves in the Poincaré sphere were chosen and are shown in Fig.(4.10). They correspond to initial states with degrees of polarization $r = 0.7 \pm 0.04$, 0.4 ± 0.01, and 0.3 ± 0.01, and normalized Stokes vectors $\hat{\boldsymbol{n}} = (0.31 \pm 0.05, 0.59 \pm 0.05, 0.75 \pm 0.04)$, $(0.71 \pm 0.03, 0.5 \pm 0.04, 0.5 \pm 0.04)$ and $(0.71 \pm 0.03, 0.5 \pm 0.04, 0.5 \pm 0.04)$. These states performed rotations about $\hat{\boldsymbol{q}} = (0, 0, 1)$, $(0.85, -0.45, -0.26)$ and $(0.31, 0.4, 0.86)$ respectively. The curves are generated by acting with $U = e^{-i\alpha \hat{\boldsymbol{q}} \cdot \boldsymbol{\sigma}}$ on the initial state, and are parametrized by $\alpha \in [0°, 180°]$ maintaining $\hat{\boldsymbol{q}}$ fixed.

Geometric phases were measured following the procedure outlined in the previous section and detection probabilities were calculated by normalizing coincidence counts with respect to a projection in the orthogonal polarization direction ($P_{|\hat{\boldsymbol{n}}\rangle\langle\hat{\boldsymbol{n}}|} = N_{|\hat{\boldsymbol{n}}\rangle\langle\hat{\boldsymbol{n}}|}/(N_{|\hat{\boldsymbol{n}}\rangle\langle\hat{\boldsymbol{n}}|} + N_{|-\hat{\boldsymbol{n}}\rangle\langle-\hat{\boldsymbol{n}}|})$, where N_k denotes the number of coincidence counts per second when projecting into state k). The measured points are shown in Fig.(4.11) and plotted against the theoretical curve. Note that although ϕ_G varies in very different ranges of values: 0.6 radians, 3 radians and 0.15 radians in Figs.(4.11a), (4.11b) and (4.11c) respectively, the agreement is very good.

Occasionally, the previously described methodology had to be modified to take into account experimental difficulties. Take for example Fig.(4.11a). Measuring the interferograms and applying Eq.(4.11) to determine the first four points on the curve gave obviously wrong results: imaginary values for ϕ_G accompanied by error bars as large as the whole graph. The problem was traced to the fact that for those specific points, the difference $1 + r - 2P_{max}$ was very close to zero and, even though theoretically it should always be positive, experimental errors turned it negative (and small). By looking at Eq.(4.11) it is clear that under such conditions an imaginary phase would be obtained (because of the square roots) and that it would be very sensible to experimental imperfections (because the slope of $\sqrt{x}$ is very large near $x = 0$). The way around this problem took advantage of the geometrical properties of ϕ_G and made use of (3.49). To obtain ϕ_G at a specific point $\rho(\alpha_1)$, the geometric phase of the complete closed curve (from $\alpha = 0°$ to $\alpha = 180°$) was measured and the solid angle it subtends determined (through (3.48)). Then, the geometric phase of the reverse curve (from $\alpha = 180°$ to $\alpha = \alpha_1$) was measured and related to the solid angle it subtends when closed by a geodesic. As can be seen from Fig.(4.12), this determines the solid angle subtended by the curve whose geometric phase is of interest. From this two solid angles, ϕ_G can be inferred. Fig.(4.11c) suffered from the same problems, but the procedure developed for Fig.(4.11a) could not be applied because the geometric phase of the reverse curve was very sensitive to experimental imperfections as well. Instead, the curve was traversed twice and the contribution

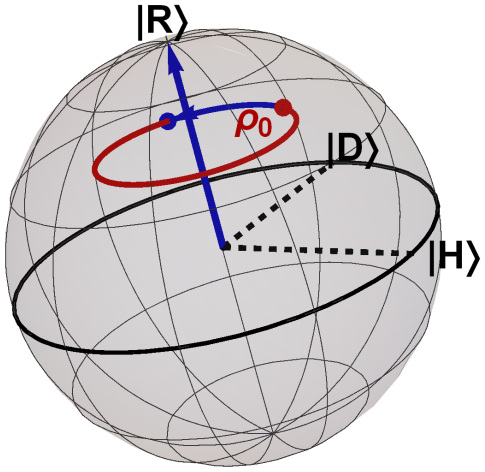

(a) Axis of rotation: $\hat{q} = (0, 1, 1)$

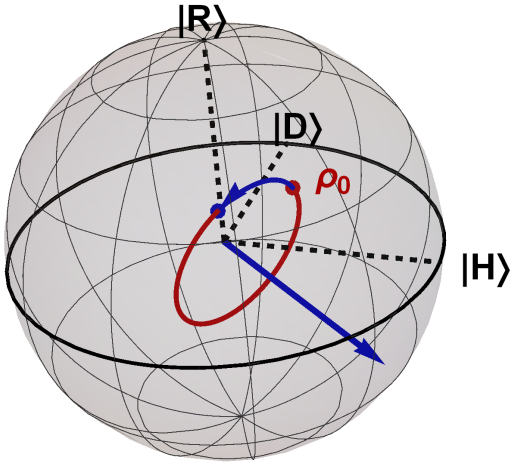

(b) Axis of rotation: $\hat{q} = (0.85, -0.45, -0.26)$

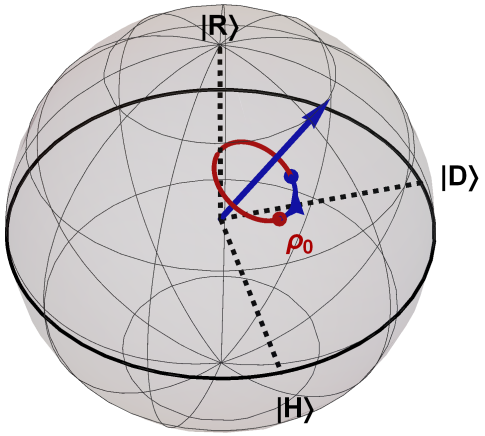

(c) Axis of rotation: $\hat{q} = (0.31, 0.4, 0.86)$

Figure 4.10: Curves followed by the state in the Poincaré sphere as it evolves under the action of $U(\alpha)$. $|H\rangle$, $|D\rangle$ and $|R\rangle$ stand for horizontal, diagonal and right-handed circular polarization, respectively.

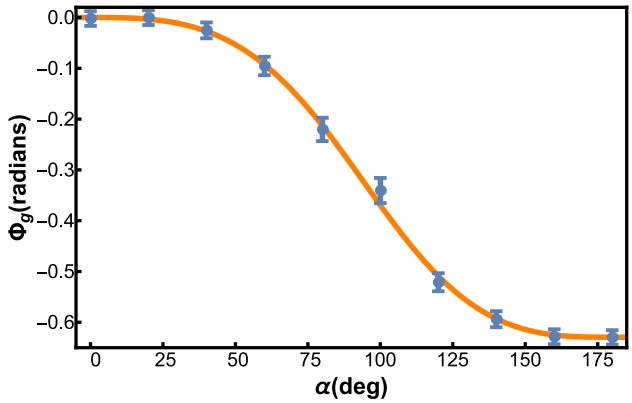

(a)

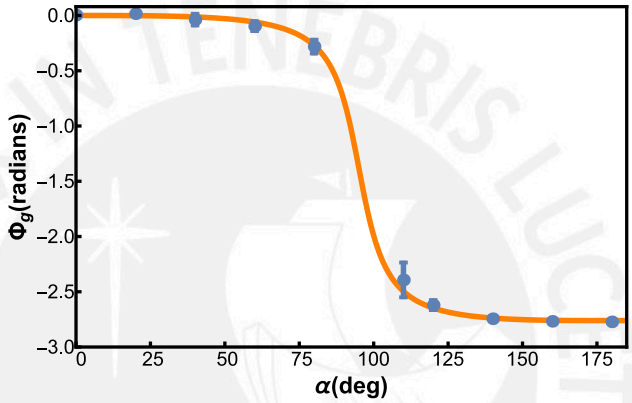

(b)

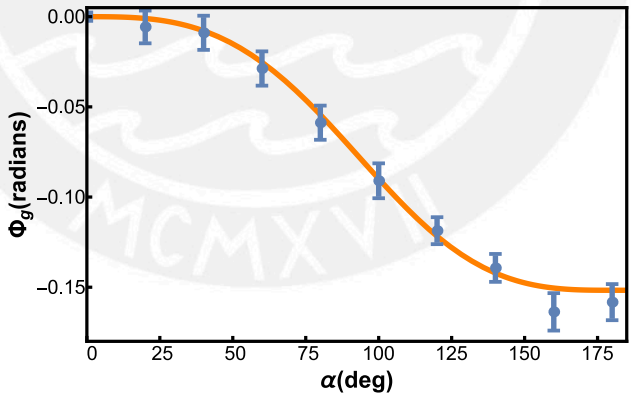

(c)

Figure 4.11: Geometric phases as functions of the evolution parameter (α) for three different initial mixed states and evolutions. The experimentally measured values (dots) are shown with their error bars. They closely agree with theoretical prediction (solid curves). The curves correspond to the evolutions shown in Fig.(4.10), respectively. (a) Initial state: $r = 0.7 \pm 0.04$, $\hat{\boldsymbol{n}} = (0.31 \pm 0.05, 0.59 \pm 0.05, 0.75 \pm 0.04)$. Axis of rotation: $\hat{\boldsymbol{q}} = (0, 0, 1)$. (b) Initial state: $r = 0.4 \pm 0.01$, $\hat{\boldsymbol{n}} = (0.71 \pm 0.03, 0.5 \pm 0.04, 0.5 \pm 0.04)$. Axis of rotation: $\hat{\boldsymbol{q}} = (0.85, -0.45, -0.26)$. (c) Initial state: $r = 0.3 \pm 0.01$, $\hat{\boldsymbol{n}} = (0.71 \pm 0.03, 0.5 \pm 0.04, 0.5 \pm 0.04)$. Axis of rotation: $\hat{\boldsymbol{q}} = (0.31, 0.4, 0.86)$.

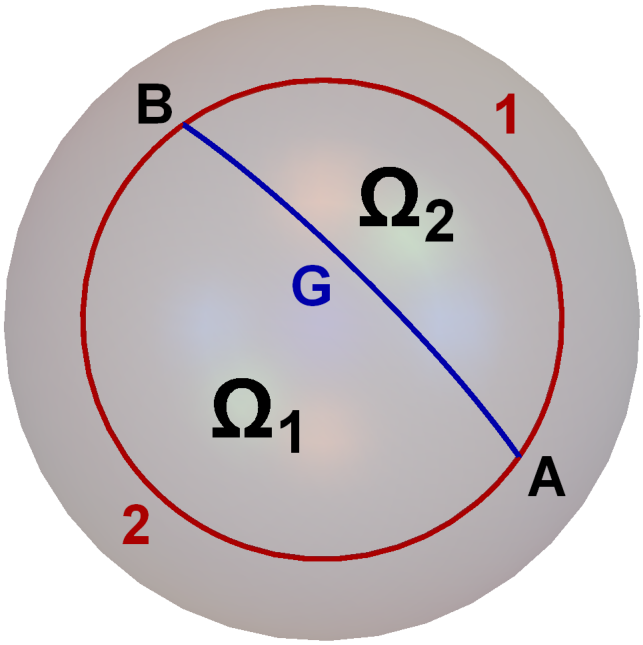

Figure 4.12: The geometric phase acquired while following path A1B is directly related to solid angle Ω_2. This solid angle can also be found as the total solid angle enclosed by path A2B1A minus Ω_1. These solid angles determine the geometric phase accumulated along paths A2B1A and A2B, respectively. Path AGB is a geodesic (great circle) that closes the open curves A1B and A2B.

from the first loop was subtracted. In the case case of Fig.(4.11b), sensitivity was found between $\alpha = 75°$ and $\alpha = 100°$ and is manifest in the large gradient around those values. This time the expression $2P_{min} - 1 + r$ was close to zero, no way to circumvent the problem was found and no reliable measurement was obtained.

Error analysis

First of all, the preparation stage involves many imperfect reflective elements (BS, PBS) which could affect the degree of polarization of the input state. To make sure that the experimentally prepared state corresponded to the desired one, full polarization state tomography was performed by measuring the Stokes parameters and the array was adjusted until the generated and target states coincided. The reported experimental errors in r and $\hat{\boldsymbol{n}}$ are due to the 1° precision of the wave plates and polarizer used to do the tomography. Once this was done, the error bars shown in Fig.(4.11) were calculated by considering each wave plate, polarizer, mirror, BS and PBS as an independent source of error and using the standard formula for error propagation $\sigma^2_{I([\theta_i])} = \sum_i (\frac{\partial I}{\partial \theta_i})^2 (\sigma_{\theta_i})^2$. Strictly speaking it should not be applicable because this would require resetting the whole array at least 30 times for each point in each interferogram, making the data recording procedure too demanding. The correct formula in the particular case of this experiment is $\sigma_{I([\theta_i])} = \sum_i |\frac{\partial I}{\partial \theta_i}| \sigma_{\theta_i}$. Nevertheless, it was numerically found that the difference between both expressions affected only non-significant digits so, for this specific case, the distinction is irrelevant. Finally, the propagated error was combined in quadrature with the errors associated to the measurement apparatus itself.

Chapter 5

Summary and Conclusions

In this Thesis we have addressed various topics. First, we have analysed and described the polarization states that routinely appear in Quantum Optics in terms of the standard description of the Electromagnetic Field: occupation number of each mode of the field. On the basis of these building blocks, polarization mixed states were defined and their basic properties and ways of representation described. In that same chapter, laser polarization was discussed in terms of the quantum states that describe it and an object, the polarization matrix, that encodes all this polarization information was introduced. Finally, the known parallel between the mixed states and the polarization matrix was shown, justified and developed.

Then, the different phases with which we had to work were described. Pancharatnam's phase was motivated by a specific interferometric setup, whereas Berry's phase was defined following the original derivation. In a more modern approach, Berry's phase was then shown to be a special case of a more general quantity, commonly called the geometric phase. The different properties of the latter were described, including its behaviour under composition of curves, characteristics for open and closed curves, and its relation to geodesics in what is known as projective space. This allowed a more profound understanding of the two-state systems with which we are concerned here. Afterwards, the same kind of analysis was done for geometric phases of mixed states undergoing unitary evolution following one of the two definitions that exist for this case.

Finally, the main experiments reported in this Thesis were described. The first one was about the generation of an arbitrary partially polarized laser source with a setup that, by virtue of the parallel described in Chapter 2, allowed the preparation of arbitrary one photon polarization mixed states as well. This array, in turn, was used as a preparation stage for a more general setup that made the initial state evolve, thereby developing a geometric phase, and then measured this acquired phase. To

achieve this, all the properties described in Chapter 3 were used: gauge invariance allowed the Pancharatnam phase to become equal to the geometric phase and properties under curve addition were used to measure experimentally problematic points. Three different curves in the Poincaré sphere were chosen and in them eight points were selected. Geometric phases acquired as the state evolved from the initial point to each one of those eight points were measured.

The array does demonstrate its capabilities since almost arbitrary curves were selected showing geometric phases that varied in very different ranges. In particular, one of them approached zero with decreasing radius whereas another one approached a step function (from 0 to π) showing completely different behaviours for states close to the maximally mixed.

While the present method to generate and measure geometric phases does not lend itself to the implementation in real time of a quantum logic gate, it does provide a way to experimentally show the effects of decoherence and other kinds of noise in these polarization geometric phases. A future line of inquiry could try to study the effect of controllable non unitary evolutions, perhaps by the use of entangled photon sources thereby gaining the ability to simulate environment induced processes.

Appendix A

Calculation of Eq.(4.8)

Eq. (4.8) for $P(\phi)$ was given without calculation. Here we derive it. We first state what is to demonstrated in Eqs.(A.1) and (A.2)

$$\begin{aligned} U_{int} &= U_{BS}U^{\dagger}_{phase}(\phi^*)U_P U_{phase}(\phi^*)U_{BS} \\ P(\phi^*) &= \langle \hat{\boldsymbol{n}}|U_{int}\rho(s_i)U^{\dagger}_{int}|\hat{\boldsymbol{n}}\rangle \end{aligned} \tag{A.1}$$

$$P = \frac{1+r}{2}\cos(\alpha)^2 + \frac{1-r\cos(\theta)^2}{2}\sin(\alpha)^2 + \frac{r}{2}\sin(\alpha)^2\sin(\theta)^2\cos(2\phi^* - 2\varphi) \tag{A.2}$$

Working in the basis of $|\hat{\boldsymbol{n}}\rangle$ and $|-\hat{\boldsymbol{n}}\rangle$, the operators take the forms shown in (A.3).

$$\begin{aligned} U_{BS} &= \frac{1}{\sqrt{2}}\begin{pmatrix} 1 & 1 \\ 1 & -1 \end{pmatrix} \\ U_{phase}(\phi^*) &= \begin{pmatrix} e^{-i\phi^*/2} & 0 \\ 0 & e^{i\phi^*/2} \end{pmatrix} \\ U_P &= e^{-i\alpha\hat{\boldsymbol{q}}\cdot\boldsymbol{\sigma}} \\ &= \begin{pmatrix} \cos(\alpha) - i\hat{\boldsymbol{q}}\cdot\hat{\boldsymbol{n}}\sin(\alpha) & -iq_c\sin(\alpha) \\ -iq_c^*\sin(\alpha) & \cos(\alpha) + i\hat{\boldsymbol{q}}\cdot\hat{\boldsymbol{n}}\sin(\alpha) \end{pmatrix} \\ q_c &= q_a^T - iq_b^T \\ \boldsymbol{q^T} &= \hat{\boldsymbol{q}} - (\hat{\boldsymbol{q}}\cdot\hat{\boldsymbol{n}})\hat{\boldsymbol{n}} \end{aligned} \tag{A.3}$$

The a and b directions are orthogonal to $\hat{\boldsymbol{n}}$ and $(\hat{\boldsymbol{a}}, \hat{\boldsymbol{b}}, \hat{\boldsymbol{n}})$ form an orthogonal triad. Things can be further simplified (A.4).

$$\begin{aligned}
\hat{\boldsymbol{q}} \cdot \hat{\boldsymbol{n}} &= \cos(\theta) \\
q_c = |q_c| e^{-i\beta} &= \left(\sqrt{(q_a^T)^2 + (q_b^T)^2} \right) e^{-i\beta} \\
&= \left(\sqrt{1 - (\hat{\boldsymbol{q}} \cdot \hat{\boldsymbol{n}})^2} \right) e^{-i\beta} = |\sin(\theta)| e^{-i\beta} \\
&= \sin(\theta) e^{-i\varphi}
\end{aligned}$$

$$U_P = \begin{pmatrix} \cos(\alpha) - i\cos(\theta)\sin(\alpha) & -i\sin(\theta)\sin(\alpha)e^{-i\varphi} \\ -i\sin(\theta)\sin(\alpha)e^{+i\varphi} & \cos(\alpha) + i\cos(\theta)\sin(\alpha) \end{pmatrix} \tag{A.4}$$

Because $\rho(s_i) = \frac{1+r}{2}|\hat{\boldsymbol{n}}\rangle\langle\hat{\boldsymbol{n}}| + \frac{1-r}{2}|-\hat{\boldsymbol{n}}\rangle\langle-\hat{\boldsymbol{n}}|$ in (A.1), the only things that should be calculated are $a = \langle\hat{\boldsymbol{n}}|U_{int}|\hat{\boldsymbol{n}}\rangle$ and $b = \langle\hat{\boldsymbol{n}}|U_{int}|-\hat{\boldsymbol{n}}\rangle$. From these, $P = \frac{1+r}{2}|a|^2 + \frac{1-r}{2}|b|^2$. Furthermore, $|a|^2 + |b|^2 = 1$ because of unitarity, so we only need to calculate a. The complete expression for a is shown in (A.5).

$$\begin{aligned}
a = &\begin{pmatrix} 1 & 0 \end{pmatrix} \frac{1}{\sqrt{2}} \begin{pmatrix} 1 & 1 \\ 1 & -1 \end{pmatrix} \begin{pmatrix} e^{i\phi^*/2} & 0 \\ 0 & e^{-i\phi^*/2} \end{pmatrix} * \\
&\begin{pmatrix} \cos(\alpha) - i\cos(\theta)\sin(\alpha) & -i\sin(\theta)\sin(\alpha)e^{-i\varphi} \\ -i\sin(\theta)\sin(\alpha)e^{+i\varphi} & \cos(\alpha) + i\cos(\theta)\sin(\alpha) \end{pmatrix} * \\
&\begin{pmatrix} e^{-i\phi^*/2} & 0 \\ 0 & e^{i\phi^*/2} \end{pmatrix} \frac{1}{\sqrt{2}} \begin{pmatrix} 1 & 1 \\ 1 & -1 \end{pmatrix} \begin{pmatrix} 1 \\ 0 \end{pmatrix} \\
= &\begin{pmatrix} \frac{e^{i\phi^*/2}}{\sqrt{2}} & \frac{e^{-i\phi^*/2}}{\sqrt{2}} \end{pmatrix} \begin{pmatrix} \cos(\alpha) - i\cos(\theta)\sin(\alpha) & -i\sin(\theta)\sin(\alpha)e^{-i\varphi} \\ -i\sin(\theta)\sin(\alpha)e^{+i\varphi} & \cos(\alpha) + i\cos(\theta)\sin(\alpha) \end{pmatrix} \begin{pmatrix} \frac{e^{-i\phi^*/2}}{\sqrt{2}} \\ \frac{e^{i\phi^*/2}}{\sqrt{2}} \end{pmatrix} \\
a = &\cos(\alpha) - i\sin(\theta)\sin(\alpha)\cos(\phi^* - \varphi)
\end{aligned} \tag{A.5}$$

From this result, both $|a|^2$ and $|b|^2$ can be obtained.

$$\begin{aligned}
|a|^2 &= \cos(\alpha)^2 + \sin(\alpha)^2\sin(\theta)^2\cos(\phi^* - \varphi)^2 \\
|b|^2 &= 1 - |a|^2 = 1 - \cos(\alpha)^2 - \sin(\alpha)^2\sin(\theta)^2(1 - \sin(\phi^* - \varphi)^2) \\
&= \sin(\alpha)^2 - \sin(\alpha)^2\sin(\theta)^2 + \sin(\alpha)^2\sin(\theta)^2\sin(\phi^* - \varphi)^2 \\
&= \sin(\alpha)^2\cos(\theta)^2 + \sin(\alpha)^2\sin(\theta)^2\sin(\phi^* - \varphi)^2
\end{aligned}$$

The final result is then (A.6)

$$
\begin{aligned}
P &= \frac{1+r}{2}|a|^2 + \frac{1-r}{2}|b|^2 \\
&= \frac{1}{2} + \frac{r}{2}(|a|^2 - |b|^2) \\
&= \frac{1}{2} + \frac{r}{2}\left(\cos(\alpha)^2 - \sin(\alpha)^2\cos(\theta)^2 + \sin(\alpha)^2\sin(\theta)^2\cos(2\phi^* - 2\varphi)\right) \\
P &= \frac{1+r}{2}\cos(\alpha)^2 + \frac{1-r\cos(\theta)^2}{2}\sin(\alpha)^2 + \frac{r}{2}\sin(\alpha)^2\sin(\theta)^2\cos(2\phi^* - 2\varphi) \quad \text{(A.6)}
\end{aligned}
$$

This is what we set out to demonstrate.

Bibliography

[1] M. V. Berry, *Quantal phase factors accompanying adiabatic changes*, Proceedings of the Royal Society of London A: Mathematical, Physical and Engineering Sciences **392** (1984), 45–57.

[2] P. Zanardi and M. Rasetti, *Holonomic quantum computation*, Physics Letters A **264** (1999), 94 – 99.

[3] P. J. Leek, J. M. Fink, A. Blais, R. Bianchetti, M. Göppl, J. M. Gambetta, D. I. Schuster, L. Frunzio, R. J. Schoelkopf, and A. Wallraff, *Observation of berry's phase in a solid-state qubit*, Science **318** (2007), 1889–1892.

[4] J. Klepp, S. Sponar, S. Filipp, M. Lettner, G. Badurek, and Y. Hasegawa, *Observation of nonadditive mixed-state phases with polarized neutrons*, Phys. Rev. Lett. **101** (2008), 150404.

[5] O. Ortíz, Y. Yugra, A. Rosario, J. C. Sihuincha, J. C. Loredo, M. V. Andrés, and F. De Zela, *Polarimetric measurements of single-photon geometric phases*, Phys. Rev. A **89** (2014), 012124.

[6] S. Berger, M. Pechal, A. A. Abdumalikov, C. Eichler, L. Steffen, A. Fedorov, A. Wallraff, and S. Filipp, *Exploring the effect of noise on the berry phase*, Phys. Rev. A **87** (2013), 060303.

[7] D. Hsieh, Y. Xia, L. Wray, D. Qian, A. Pal, J. H. Dil, J. Osterwalder, F. Meier, G. Bihlmayer, C. L. Kane, Y. S. Hor, R. J. Cava, and M. Z. Hasan, *Observation of unconventional quantum spin textures in topological insulators*, Science **323** (2009), 919–922.

[8] J. Dalibard, F. Gerbier, G. Juzeliūnas, and P. Öhberg, *Colloquium : Artificial gauge potentials for neutral atoms*, Rev. Mod. Phys. **83** (2011), 1523–1543.

[9] M. Ericsson, D. Achilles, J. T. Barreiro, D. Branning, N. A. Peters, and P. G. Kwiat, *Measurement of geometric phase for mixed states using single photon interferometry*, Phys. Rev. Lett. **94** (2005), 050401.

[10] B.-G. Englert, C. Kurtsiefer, and H. Weinfurter, *Universal unitary gate for single-photon two-qubit states*, Phys. Rev. A **63** (2001), 032303.

[11] M. Born and E. Wolf, *Principles of Optics*, Cambridge University, 1999.

[12] E. Sjöqvist, A. K. Pati, A. Ekert, J. S. Anandan, M. Ericsson, D. K. L. Oi, and V. Vedral, *Geometric phases for mixed states in interferometry*, Phys. Rev. Lett. **85** (2000), 2845–2849.

[13] S. Pancharatnam, *Generalized theory of interference, and its applications*, Proceedings of the Indian Academy of Sciences - Section A **44** (1956), 247–262.

[14] A. Shapere and F. Wilczek, *Geometric Phases in Physics*, World Scientific Publishing Co. Pte. Ltd., 1989.

[15] S.-L. Zhu and Z. D. Wang, *Unconventional geometric quantum computation*, Phys. Rev. Lett. **91** (2003), 187902.

[16] J. A. Jones, V. Vedral, A. Ekert, and G. Castagnoli, *Geometric quantum computation using nuclear magnetic resonance*, Nature **403** (2000), 869–871.

[17] E. Sjöqvist, *Geometric phases in quantum information*, International Journal of Quantum Chemistry **115** (2015), 1311–1326.

[18] A. Blais and A.-M. S. Tremblay, *Effect of noise on geometric logic gates for quantum computation*, Phys. Rev. A **67** (2003), 012308.

[19] A. Nazir, T. P. Spiller, and W. J. Munro, *Decoherence of geometric phase gates*, Phys. Rev. A **65** (2002), 042303.

[20] S.-L. Zhu and P. Zanardi, *Geometric quantum gates that are robust against stochastic control errors*, Phys. Rev. A **72** (2005), 020301.

[21] D. Leibfried, B. DeMarco, V. Meyer, D. Lucas, M. Barrett, J. Britton, W. M. Itano, B. Jelenkovic, C. Langer, T. Rosenband, and D. J. Wineland, *Experimental demonstration of a robust, high-fidelity geometric two ion-qubit phase gate*, Nature **422** (2003), 412–415.

[22] S. Filipp, J. Klepp, Y. Hasegawa, C. Plonka-Spehr, U. Schmidt, P. Geltenbort, and H. Rauch, *Experimental demonstration of the stability of berry's phase for a spin-1/2 particle*, Phys. Rev. Lett. **102** (2009), 030404.

[23] P. Milman and R. Mosseri, *Topological phase for entangled two-qubit states*, Phys. Rev. Lett. **90** (2003), 230403.

[24] W. LiMing, Z. L. Tang, and C. J. Liao, *Representation of the* SO(3) *group by a maximally entangled state*, Phys. Rev. A **69** (2004), 064301.

[25] J. C. Loredo, M. A. Broome, D. H. Smith, and A. G. White, *Observation of entanglement-dependent two-particle holonomic phase*, Phys. Rev. Lett. **112** (2014), 143603.

[26] N. Mukunda and R. Simon, *Quantum kinematic approach to the geometric phase. i. general formalism*, Annals of Physics **228** (1993), 205 – 268.

[27] F. de Zela, *The pancharatnam-berry phase: Theoretical and experimental aspects*, in Theoretical Concepts of Quantum Mechanics, (M. R. Pahlavani, ed.), InTech, 2012, Chap. 14, pp. 289–312.

[28] A. Uhlmann, *Parallel transport and quantum holonomy along density operators*, Reports on Mathematical Physics **24** (1986), 229 – 240.

[29] A.-B. Mahler and R. A. Chipman, *Polarization state generator: a polarimeter calibration standard*, Appl. Opt. **50** (2011), 1726–1734.

[30] T. Shirai and E. Wolf, *Coherence and polarization of electromagnetic beams modulated by random phase screens and their changes on propagation in free space*, J. Opt. Soc. Am. A **21** (2004), 1907–1916.

[31] A. Ostrovsky, M. Olvera, C. Rickenstorff, G. MartÃnez-Niconoff, and V. Arrizón, *Generation of a secondary electromagnetic source with desired statistical properties*, Optics Communications **283** (2010), 4490 – 4493 (Electromagnetic Coherence and Polarization).

[32] A. Peinado, A. Lizana, and J. Campos, *Use of ferroelectric liquid crystal panels to control state and degree of polarization in light beams*, Opt. Lett. **39** (2014), 659–662.

[33] A. S. Ostrovsky, G. Rodríguez-Zurita, C. Meneses-Fabián, M. A. Olvera-Santamaría, and C. Rickenstorff-Parrao, *Experimental generating the partially coherent and partially polarized electromagnetic source*, Opt. Express **18** (2010), 12864–12871.

[34] D. Barberena, G. Gatti, and F. D. Zela, *Experimental demonstration of a secondary source of partially polarized states*, J. Opt. Soc. Am. A **32** (2015), 697–700.

[35] A. Lizana, I. Estévez, F. A. Torres-Ruiz, A. Peinado, C. Ramirez, and J. Campos, *Arbitrary state of polarization with customized degree of polarization generator*, Opt. Lett. **40** (2015), 3790–3793.

[36] N. A. Peters, J. T. Barreiro, M. E. Goggin, T.-C. Wei, and P. G. Kwiat, *Remote state preparation: Arbitrary remote control of photon polarization*, Phys. Rev. Lett. **94** (2005), 150502.

[37] W.-T. Liu, W. Wu, B.-Q. Ou, P.-X. Chen, C.-Z. Li, and J.-M. Yuan, *Experimental remote preparation of arbitrary photon polarization states*, Phys. Rev. A **76** (2007), 022308.

[38] A. G. White, D. F. V. James, P. H. Eberhard, and P. G. Kwiat, *Nonmaximally entangled states: Production, characterization, and utilization*, Phys. Rev. Lett. **83** (1999), 3103–3107.

[39] G. Temporao, G. Xavier, and J. von der Weid, *Quantum channel with controllable decoherence using polarization-time coupling*, Eur. Phys. J. D **66** (2012), 42:1–6.

[40] D. Barberena, O. Ortíz, Y. Yugra, R. Caballero, and F. De Zela, *All-optical polarimetric generation of mixed-state single-photon geometric phases*, Phys. Rev. A **93** (2016), 013805.

[41] A. G. Wagh and V. C. Rakhecha, *On measuring the pancharatnam phase. ii. su(2) polarimetry*, Physics Letters A **197** (1995), 112 – 115.

[42] R. Simon and N. Mukunda, *Minimal three-component su(2) gadget for polarization optics*, Physics Letters A **143** (1990), 165 – 169.